KfK 5241
September 1993

Convective-diffusive Transport in Laminar MHD Flows

L. Bühler
Institut für Angewandte Thermo- und Fluiddynamik
Projekt Kernfusion

Kernforschungszentrum Karlsruhe

Kernforschungszentrum Karlsruhe
Institut für Angewandte Thermo– und Fluiddynamik
Projekt Kernfusion

KfK 5241

Convective – diffusive transport in laminar MHD flows

L. Bühler

Kernforschungszentrum Karlsruhe GmbH, Karlsruhe

Kernforschungszentrum Karlsruhe GmbH
Postfach 3640, 76021 Karlsruhe

ISSN 0303-4003

Convective – diffusive transport in laminar MHD flows

Abstract

The two questions of main interest for the design of a fusion blanket are whether the heat transfer to the coolant is high enough that the temperature of the plasma facing wall does not exceed a critical value and whether the corrosion rate is below a certain limit. Both processes are governed by convective- diffusive transport mechanisms. A numerical code for the 3D-solution of these equations in the laminar flow regime is discussed. It is assumed that the flow is fully developed when entering the heated section of a blanket element. The interaction of the strong magnetic field with the electrically conducting fluid is taken into account by an asymptotic analysis valid for fully developed MHD flows in ducts with arbitrary shape of cross section. Heat transfer conditions are discussed for circular pipes and square ducts. The influence of the main parameters on wall temperature is analyzed in detail and summarized by an empirical correlation. As an example for an extended use of the heat transfer code the full numerical solution of fully developed MHD flows in circular and rectangular ducts is presented.

Konvektiv – diffusiver Transport in laminaren MHD Strömungen

Zusammenfassung

Bei der Auslegung eines Fusionsblankets sind die wichtigen Fragen zu klären, ob die Wärmeübertragung an das Kühlmedium ausreicht, damit die Temperatur der plasmanahen Wand einen kritischen Wert nicht übersteigt, und ob die Korrosionsraten unterhalb eines gewissen Grenzwertes bleiben. Beide Prozesse werden durch Gleichungen für konvektiv- diffusive Transportvorgänge beschrieben. Es wird ein numerisches Rechenverfahren zur Bestimmung von dreidimensionalen Lösungen dieser Gleichungen im Bereich laminarer Strömungen vorgestellt. Dabei wird vorausgesetzt, daß die Strömung beim Eintritt in den beheizten Teil des Blankets bereits voll ausgebildet ist. Die Wechselwirkung des starken Magnetfeldes mit dem elektrisch leitenden Fluid wird durch eine asymptotische Rechnung berücksichtigt, die für voll ausgebildete MHD Strömungen in Kanälen mit beliebigen Querschnitten gilt. Berechnungen zur Wärmeübertragung werden für Kreisrohre und für Kanäle mit quadratischem Querschnitt durchgeführt. Der Einfluß der wichtigsten Parameter wird in einer empirischen Korrelation zusammengefaßt. Als Beispiel für eine erweiterte Anwendung des Wärmeübertragungs– Programms wird die vollnumerische Lösung für ausgebildete MHD Strömungen in Kreisrohren und Rechteckkanälen vorgestellt.

Convective – diffusive transport in laminar MHD flows

Contents

1 Introduction

Heat transfer in magneto-hydrodynamic *(MHD)* flows plays an important role for the design of a liquid-metal cooled fusion blanket. The extremely high fusion heat flux may require enormous velocities in the vicinity of the plasma facing first wall even if the liquid metal provides excellent heat conduction.

Liquid metals are considered as cooling media for application in a fusion reactor due to their high heat conductivity. Their use, however, may cause corrosion problems. Corrosion at the surface of ferritic structure materials is dominated by a diffusive process at the fluid-wall interface (Borgstedt & Röhrig 1991) and further by convective diffusive transport in the liquid metal. The transport of thermal energy and of mass of a dissolved corrosion component are governed by the same equations and discussed, if possible, simultaneously in this report.

Another problem which has to be considered is the interaction of the electrically conducting fluid and the strong magnetic field confining the fusion plasma. MHD effects usually lead to higher pressure drop compared to hydrodynamic flows. The electromagnetic forces acting upon the moving fluid have a strong influence on the flow distribution in the cross section of a cooling channel. This may have unfavorable consequences on heat transfer in electrically insulating circular pipes, but also favorable effects at the heated side wall of electrically conducting rectangular ducts.

Heat and mass transfer in MHD flows has been analyzed in the past by several authors. In their textbook on 'Heat and Mass Transfer in MHD Flows' Blums, Mikhailov & Ozols (1987) present the governing equations and give a summary of previous works. A completely numerical approach for calculating 3D-MHD flows is outlined by Kunugi, Tillack & Abdou 1991 or by Kim & Abdou 1989. They present results for the fluid velocity in 2D- flows in infinitely long channels and in 3D-bend flow or 3D-flows in a fringing magnetic field. They concentrate their discussion of results mainly on the MHD flow variables and only minor on heat transfer conditions. Ying, Lavine & Tillack 1989 derive an analytical solution for the heat transfer across the side layer of a Hunt-type MHD flow with conducting Hartmann walls and insulating side walls. They show also results for special heat transfer problems in other fully developed MHD flows in rectangular ducts obtained on the basis of a numerical analysis (more detailed results are presented by Ying & Tillack 1991). Hua & Picologlou 1989 present an integral approach for heat transfer calculations in high velocity side layers. Comparisons with results obtained by numerical calculations show excellent agreement in the considered range of parameters.

In circular ducts fully developed heat transfer conditions have been analyzed analytically by Gardner 1967 for constant wall-normal heat flux. A similar problem has been investigated experimentally by Gotovskiy & Firsova 1992. Their main result is that heat transfer is improved if a transverse magnetic field is applied to the heated section of an electrically conducting pipe, especially at Peclet numbers $Pe<10^3$, when fully developed thermal conditions are established within the heated test section. At the end of the section the ratio of the Nusselt number for MHD flow $Nu_{Ha>0}$ and for hydrodynamic flow $Nu_{Ha=0}$ is close to the value $Nu_{Ha>0}/Nu_{Ha=0}=11/6$, which results from fully developed heat transfer in circular bulk flow (MHD flow in conducting pipes is of bulk type) $Nu_{bulk}=8$ and for hydrodynamic flow $Nu_{Ha=0}=48/11$.

This report treats the heat transfer problem for rectangular channels and for circular pipes with MHD velocity profiles which were assumed to be fully developed when the fluid enters the heated section of the blanket. The MHD flow problem is solved by an asymptotic analysis similar to Chang & Lundgren 1961 or Walker 1981 for ducts with arbitrary cross sections or for rectangular ducts, respectively. The governing equations for heat transfer are solved numerically by finite differences using an *ADI* method for the two coordinates in the plane of the cross section during successive increase of the axial position. For fusion typical consideration the heat flux is assumed to be perpendicular to the applied strong magnetic field, but also other interesting cases are discussed.

Finally an extended use of the developed numerical code is discussed for other problems which are governed by equations of heat conduction type. As an example the full numerical solution of MHD flows in conducting or non-conducting ducts of rectangular and of circular cross section is obtained just by using the heat transfer code.

2 Fully developed MHD flows

2.1 Equations and boundary conditions

MHD flows in strong magnetic fields show fully developed flow structures at relatively short distances upstream and downstream of three– dimensional disturbances (except in insulating circular pipes). Since these distances are in general much shorter than the developing length of convective– diffusive boundary layers (at high Peclet numbers; see later), fully developed MHD flow is assumed in the following analysis.

The equations governing fully developed MHD flow read in their non-dimensional form:

$$M^{-2}\nabla^2 \boldsymbol{v} + \boldsymbol{j}\times\boldsymbol{B} = \nabla p, \qquad (2.1a)$$

$$\boldsymbol{j} = -\nabla\phi + \boldsymbol{v}\times\boldsymbol{B}, \qquad (2.1b)$$

$$\nabla\cdot\boldsymbol{v} = 0, \qquad (2.1c)$$

$$\nabla\cdot\boldsymbol{j} = 0, \qquad (2.1d)$$

where the magnetic field $\boldsymbol{B}$, the fluid velocity $\boldsymbol{v}$, the electric current density $\boldsymbol{j}$, the electric potential ϕ and the pressure p are normalized by B_0 –the magnitude of the applied strong magnetic field–, v_0 –the average fluid velocity–, $\sigma v_0 B_0$, $v_0 B_0 L$ and $\sigma v_0 B_0{}^2 L$, respectively. M^2 gives the ratio of electromagnetic effects to viscous effects, where $M = B_0 L\sqrt{\sigma/\rho\nu}$ is the ***Hartmann number*** and L is a characteristic dimension of the cross section. The electric conductivity σ of the fluid and its kinematic viscosity ν are assumed to be constant.

The boundary conditions at channel walls are the no-slip condition

$$\boldsymbol{v} = \boldsymbol{0}, \qquad (2.1e)$$

and a condition for the current component normal to the walls. This can be the condition for thin conducting walls (Walker 1981) or for insulating walls

$$\boldsymbol{j}\cdot\boldsymbol{n} = \nabla_w\cdot(c\nabla_w\phi_w) \quad \text{or} \quad \boldsymbol{j}\cdot\boldsymbol{n} = 0, \qquad (2.1f,g)$$

respectively. ϕ_w is the potential at the wall and $c=\sigma_w t/\sigma L$ is the wall conductance ratio; σ_w, t are the conductivity and the thickness of the wall; ∇_w is the gradient in the plane tangential to the wall; $-\vec{j}\cdot\vec{n}$ is the current entering the wall from the fluid.

In fully developed flow the velocity vector has only one non-zero component u in the flow (the x-) direction. There is no variation of the mechanical or electrical flow variables with x and current component j_x vanishes. Currents close their circuit in the same cross section and the only non-zero component of pressure gradient $\partial_x p$ is constant everywhere.

The vector of the magnetic induction $\vec{B}=(B_x, B_y, 0)$ consists of two components. The component $B_y=1$ is given by the applied strong field, while the component B_x describes the field, which is induced by currents j_y and j_z in the cross section due to *Ampere's law* $\nabla\times\vec{B}=R_m\vec{j}$. $R_m=\mu\sigma a v_0$ is the magnetic Reynolds number, where μ is the magnetic permeability. Since there is no interaction between the induced field B_x and the fluid moving in the x-direction it is not necessary to know about B_x in detail.

At high Hartmann numbers the flow exhibits a ***core*** where the pressure gradient is mainly balanced by the electromagnetic force. Viscous effects are confined to thin boundary layers near channel walls. They are called ***Hartmann layers*** if there is a significant normal component of the applied magnetic field at the wall. Their thickness is $O(M^{-1})$. All flow variables may be expressed in terms of an solution for inviscid flow, describing the main flow in the core and in terms of boundary layer contributions accounting for viscous effects and satisfying the no-slip condition *(2.1e)*.

2.2 MHD flows in ducts of arbitrary symmetric cross section

The equations governing fully developed MHD flow in the core and in the Hartmann layers can be considered without any reference to the shape of the duct's cross section. For large Hartmann numbers ($M=10^3$-10^5 for fusion applications) the equations *(2.1a-d)* reduce to

$$\partial_x p_C = -j_{z,C} = \partial_z \phi_C - u_C \,, \qquad (2.2a,b)$$

$$j_{y,C} = -\partial_y \phi_C = 0 \,, \qquad (2.2c,d)$$

in the core and additional contributions in the Hartmann layer

$$\partial_{\eta\eta} u_\delta - u_\delta = 0 \,, \qquad (2.2e)$$

$$p_\delta = 0, \; \phi_\delta = 0 \,. \qquad (2.2f,g)$$

$\eta = M(y-h)$ is the stretched boundary layer coordinate and $y = \pm h(z)$ gives the y--position of the duct wall at any value of z. It represents the shape of an arbitrary, but symmetric duct. The core velocity $u_C = u_C(z)$ is a function of z, only.

The total velocity $u = u_C + u_\delta$ is

$$u = u_C(z)\left[1 - e^{M(y-h)}\right] \qquad (2.2h)$$

(see for example Moreau 1990, p.125).

Conservation of charge at any position z_0 may be expressed by

$$\int_0^h j_z dy - c\partial_t \phi_w = 0. \qquad (2.2i)$$

The integral gives the total current inside the fluid. The second term represents currents inside the channel wall. See figure 2.1. Since there is no variation of potential across the Hartmann layer *(2.2g)*, (according to the approximation at high Hartmann numbers) the wall potential is equal to the potential of the core, $\phi_w = \phi_C$. t is the coordinate tangential to the duct wall. The derivative with respect to the tangential direction can be replaced by a derivative with respect to the z-direction.

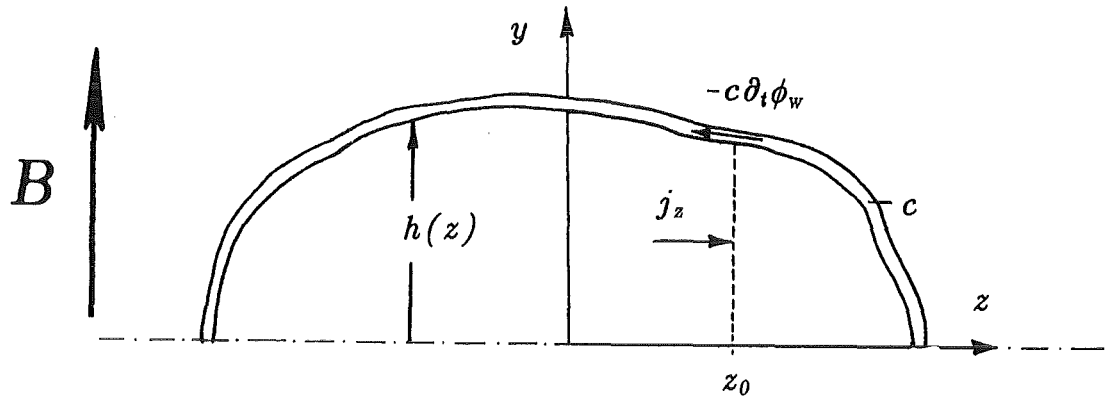

Figure 2.1 Geometry of an arbitrary symmetric duct

After integration equation *(2.2i)* reads

$$-h\partial_z\phi_C + u_C(h - \frac{1}{M}) - \frac{c}{\sqrt{1+(\partial_z h)^2}}\,\partial_z\phi_C = 0\ . \qquad (2.2j)$$

A relation between the core velocity and the constant pressure gradient is obtained by eliminating $\partial_z\phi_C$ from *(2.2b)* and *(2.2j)*.

$$u_C(z) = -\,\partial_x p\,\frac{c + h\sqrt{1+(\partial_z h)^2}}{c + \frac{1}{M}\sqrt{1+(\partial_z h)^2}}\ . \qquad (2.2k)$$

This equation shows some interesting limiting cases:

- The core velocity does not vary with z and is equal to the negative pressure gradient if the channel walls are perfect conductors $(c\longrightarrow\infty)$.
- The core velocity is proportional to the channel height $h(z)$ if walls are insulating $(c=0)$. The velocity profile is directly given by the channel geometry only.
- If the Hartmann number is very high $(M>>\sqrt{1+(\partial_z h)^2})$ the flow exhibits regions of extremely high velocities if a part of the duct wall becomes almost parallel to the applied magnetic field $(\partial_z h\longrightarrow\infty)$. Flows in ducts with walls exactly aligned with the field can not be calculated by equation *(2.2k)*. However, if the parallel walls are slightly deformed the above equation holds for the velocity in the core and accounts precisely for the volume flux carried by high-velocity layer. (In this case the additional volume flux in parallel layers, Q_p, is already covered and has not to be calculated separately as shown in equation *(2.2l)* below.)

Equation *(2.2k)* was already derived by Chang & Lundgren (1961). Their calculation was based on relations between the induced magnetic field and the velocity, while the present analysis uses relations between velocity and potential.

A normalization of the total volume flux

$$\int_{z_{min}}^{z_{max}}(h - \frac{1}{M})\,u_C(z)\,dz + Q_p = \int_{z_{min}}^{z_{max}} h\,dz \qquad (2.2l)$$

determines finally the pressure gradient $\partial_x p$. Q_p is the volume flux carried by layers

parallel to the magnetic field. Such layers appear at walls exactly parallel to the magnetic field (for example in rectangular ducts where they are called the ***side layers***).

2.3 Velocity distribution and pressure drop in circular pipes

MHD flows in ducts with circular cross section are considered first, because they are widely used in technical applications. An analytical solution for MHD flows in circular ducts is given by Gold 1962. A detailed asymptotic analysis (Roberts 1967) shows that near the two singular points, where the magnetic field lines are tangential to the duct wall, another type of boundary layer appears (the ***Roberts layers***). Their thickness is $O(M^{-2/3})$ and the extension in magnetic field direction is $O(M^{-1/3})$. Since these layers are restricted to very narrow regions and do not carry an $O(1)$ volume flux ($Q_p=0$) they are unimportant for the flow outside and not considered in the following analysis.

The above introduced theory for flows in arbitrary geometries can be used to calculate the flow structure in the whole duct. The circular cross section is defined by

$$h = \sqrt{1-z^2}\,. \qquad (2.3a)$$

As $z \longrightarrow 1$, $\partial_z h$ tends to infinity, h tends to zero and u_C reaches a finite limit. The region, where the magnetic field is parallel to duct walls is restricted to two singular points in a cross section.

Equation $(2.2k)$ reduces to

$$u_C(z) = -\,\partial_x p\,\frac{c + 1}{c + \frac{1}{Mh}}\,. \qquad (2.3b)$$

The pressure drop is found by equation $(2.2l)$ to be

$$\partial_x p = \frac{\frac{1}{2}\pi}{\int_{-1}^{1} \frac{(h-1/M)(c+1)}{c + 1/Mh}\,dz}\,, \qquad (2.3c)$$

where the integral can be evaluated to

$$\int_{-1}^{1}(\ldots)\,dz = \tfrac{1}{2}\pi\,\frac{c+1}{c} + \frac{(1+c)^2}{M^2c^3}\left[\pi - 2Mc + \frac{4}{a}\arctan\frac{Mc-1}{a}\right], \qquad (2.3d)$$

with $a=\sqrt{1-M^2c^2}$.

The influence of the wall conductance ratio on pressure gradient is shown in figure 2.2a. For a highly conducting wall ($c>>M^{-1}$) the pressure drop tends to the asymptotic value of $\partial_x p=-c/(1+c)$ for all Hartmann numbers. If the duct wall is a poor conductor ($c<<M^{-1}$) the pressure gradient tends to $\partial_x p=-3\pi/8M$ as given by Gold 1962.

Velocity profiles obtained by *(2.3b)* are shown in figure 2.2b for a Hartmann number $M=1000$ and several values of the wall conductance ratio c.

Fully developed velocity profiles obtained by a numerical solution of full induction-less MHD equations in circular pipe geometry is shown in figure 6.2.

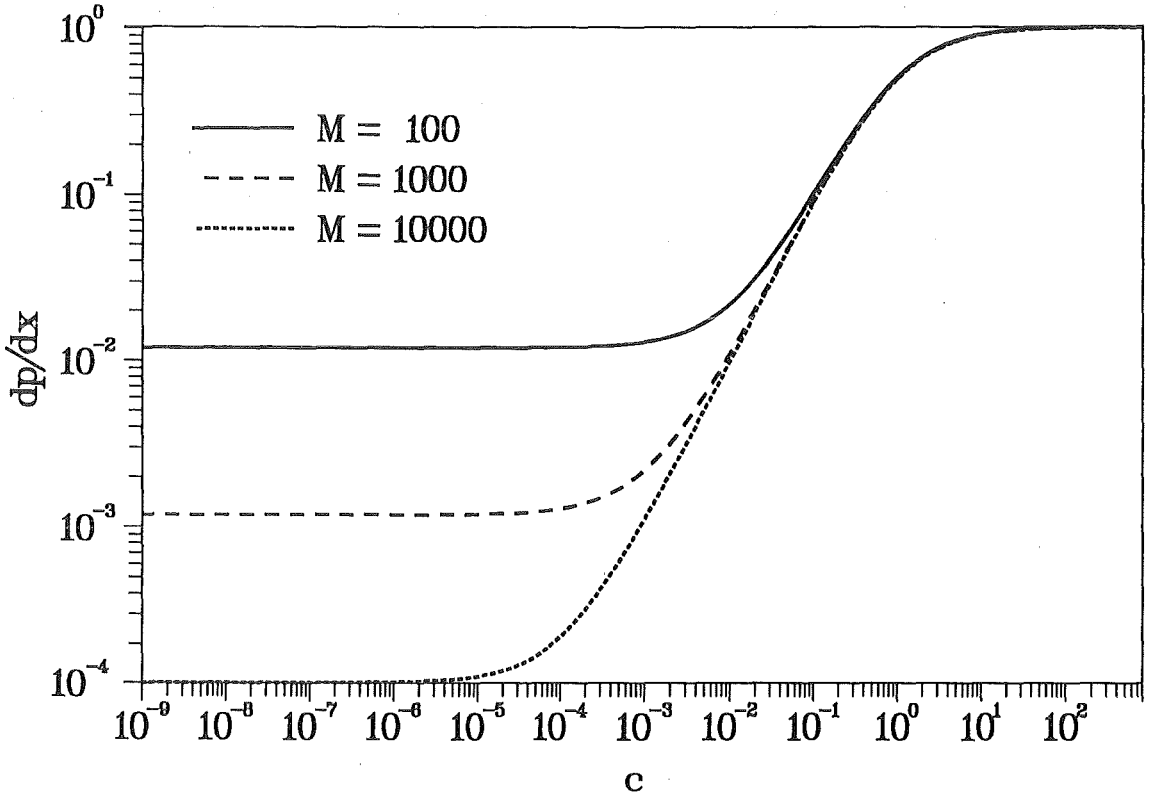

Figure 2.2a *MHD-Pressure drop in a circular pipe for different Hartmann numbers as a function of the wall conductance ratio.*

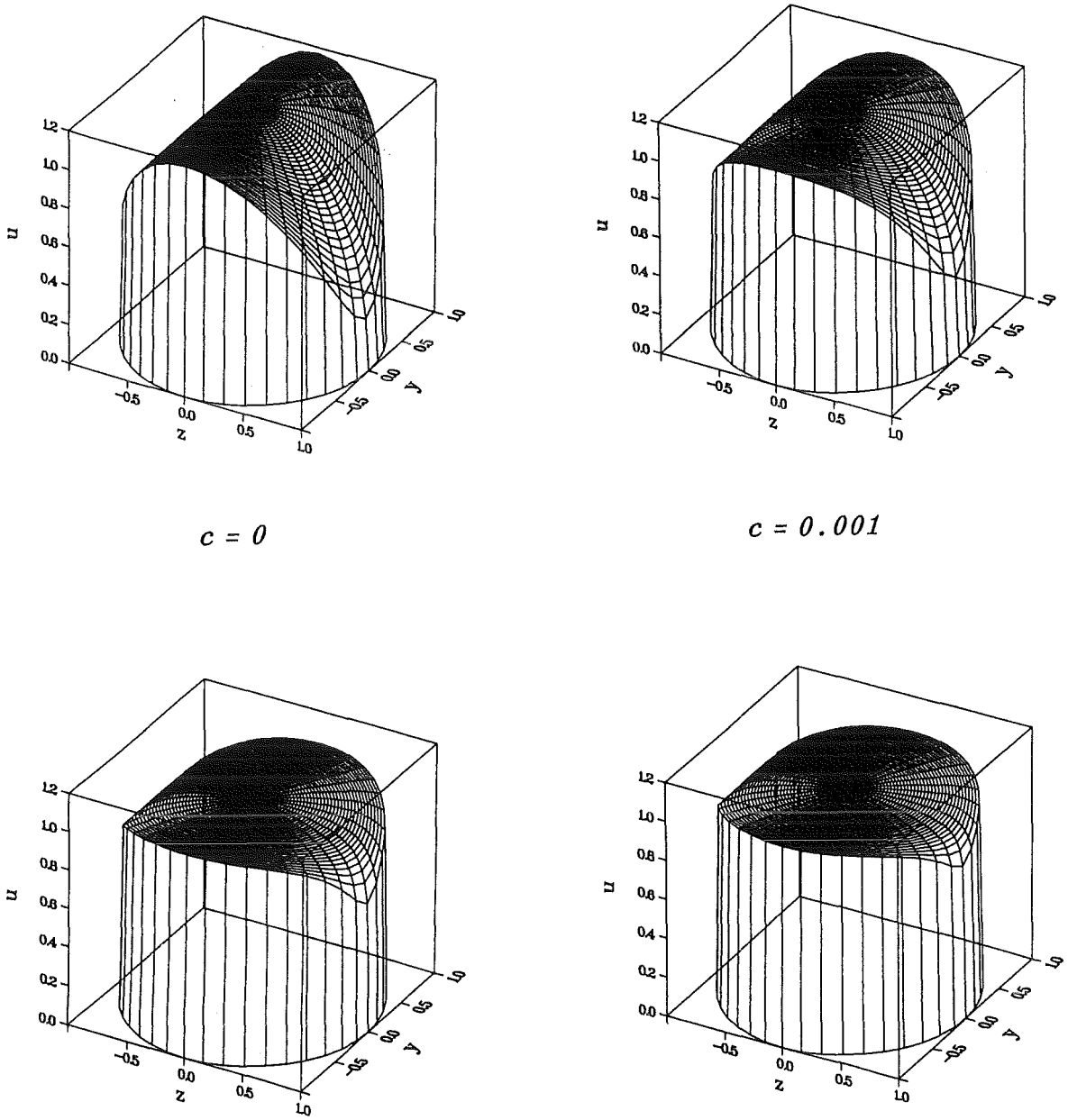

Figure 2.2b *MHD-velocity profiles in a circular pipe for different wall conductance ratios at a Hartmann number M=1000.*

2.4 Velocity distribution and pressure drop in rectangular ducts

The considered rectangular geometry is bounded by two walls perpendicular to the applied field at $y=\pm 1$, $(h=\pm 1)$ called the ***Hartmann walls***, and by two walls parallel to the field at $z=\pm b$, called the ***side walls*** (see figure 2.3).

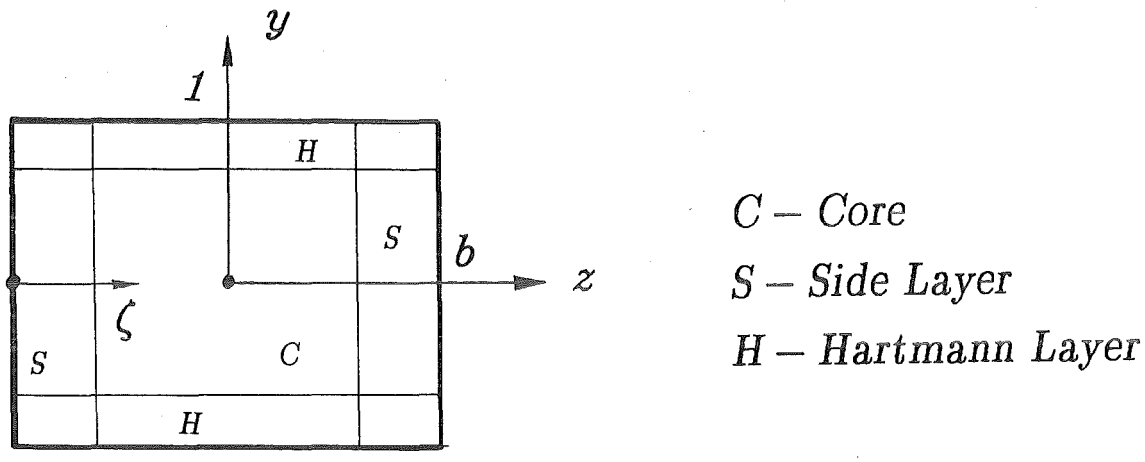

Figure 2.3 Geometry of a rectangular duct.

For strong magnetic fields $(M>>1)$ the analysis described in §2.2 holds for the flow in the core and in Hartmann layers. Near the side walls the basic equations may be reduced to a single equation for the additional side layer contribution ϕ_S to the potential.

$$\partial_{yy}\phi_S = \partial_{\zeta\zeta\zeta\zeta}\phi_S \ . \qquad (2.4a)$$

$\zeta=\sqrt{M}(b-z)$ or $\zeta=\sqrt{M}(b+z)$ is the stretched side layer coordinate at the walls $z=b$ and $z=-b$, respectively. The solution of $(2.4a)$ in form of Fourier series reads (see Walker 1981)

$$\phi_S = \sum_{i=1}^{\infty} e^{-\alpha_i\zeta}\left[A_{1,i}\cos\alpha_i\zeta + A_{2,i}\sin\alpha_i\zeta \right] \cos\beta_i y \ , \qquad (2.4b)$$

with $\beta_i = \frac{1}{2}\pi(2i-1)$ and $\alpha_i = \sqrt{\frac{1}{2}\beta_i}$.

If the conductance ratio of the side walls c_S is high enough $(c_S>>M^{-\frac{1}{2}})$ current passes the side layer unchanged in z-direction $(j_z=j_{zC},\ j_{zS}=0)$. The additional side layer contribution u_S to the velocity is then obtained by the use of $(2.1b)$ and $(2.4b)$.

$$u_S = \sum_{i=1}^{\infty} e^{-\alpha_i \zeta}\left[B_{1,i}\cos\alpha_i\zeta + B_{2,i}\sin\alpha_i\zeta \right] \cos\beta_i y \ . \qquad (2.4c)$$

The coefficients $A_{1,i}$ are calculated via boundary condition $(2.1f)$ at $\zeta=0$ in the form of

$$j_{zC} = -\partial_x p = c_S \sum_{i=1}^{\infty} \beta_i{}^2 A_{1,i}\cos\beta_i y \qquad (2.4d)$$

as

$$A_{1,i} = (-1)^i \frac{2}{\beta_i{}^3}\frac{\partial_x p}{c_s} \ . \qquad (2.4e)$$

The coefficients $B_{1,i}$ are obtained from the non–slip condition $(2.1e)$ at $\zeta=0$ in form of

$$u_S = -u_C = \sum_{i=1}^{\infty} B_{1,i}\cos\beta_i y \ , \qquad (2.4f)$$

as

$$B_{1,i} = (-1)^i \frac{2}{\beta_i} u_C \ . \qquad (2.4g)$$

The coefficients $B_{2,i}$ are determined due to Ohms's law $-\sqrt{M}\partial_\zeta \phi_S + u_S = O(M^{-\frac{1}{2}})$ as

$$B_{2,i} = -B_{1,i} + 2\sqrt{M}\alpha_i A_{1,i} \ . \qquad (2.4h)$$

The additional volume flux condition carried by the parallel layers in the upper half of the channel is

$$Q_p = 2\int_0^1 \int_0^{\infty} u_S(y,\zeta)\, d\zeta\, dy = -2\frac{\partial_x p}{c_s} \sum_{i=1}^{\infty} \frac{2}{\beta_i{}^4} \ . \qquad (2.4i)$$

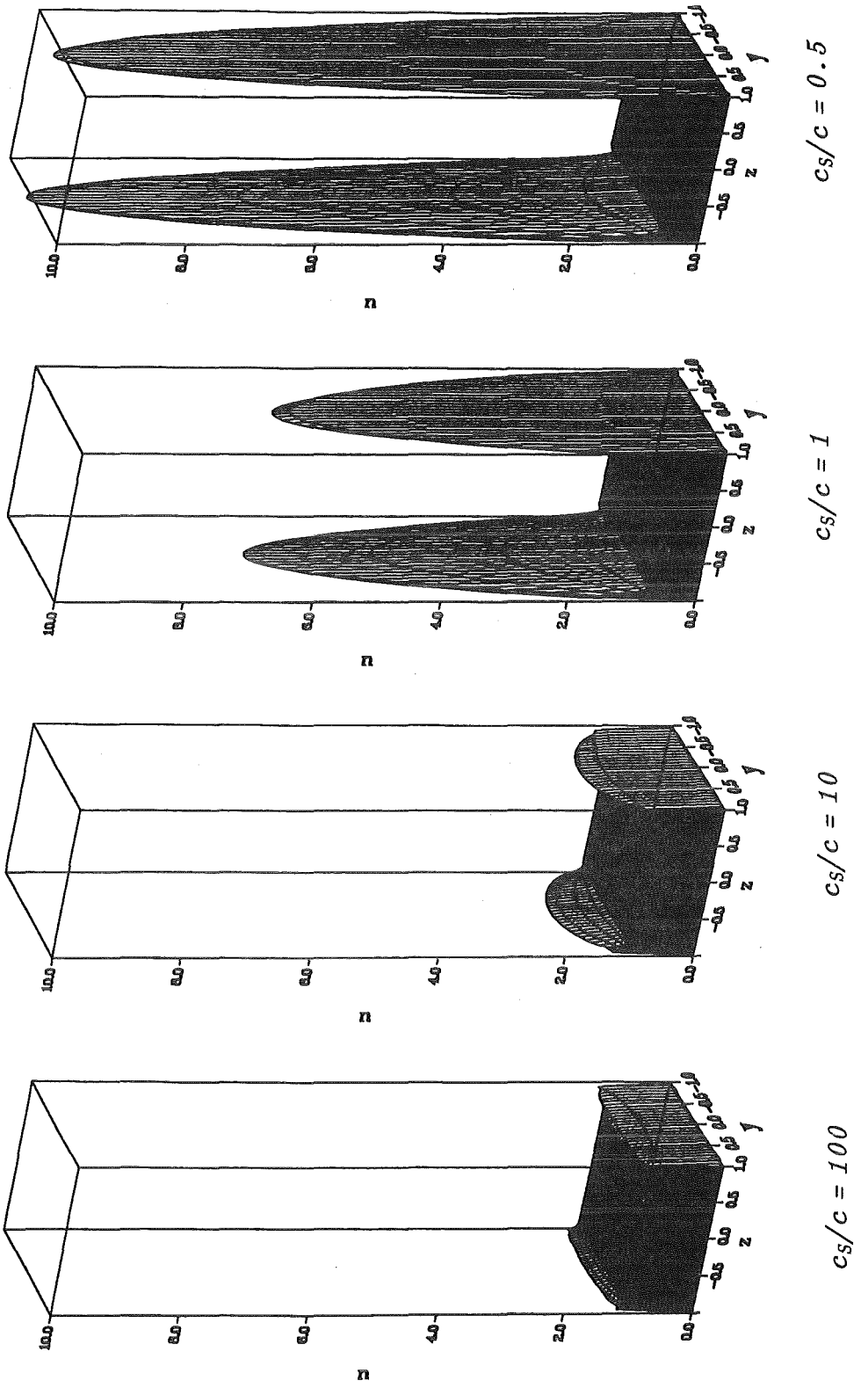

Figure 2.4 *MHD-velocity profiles in a square duct for different ratios c_S/c at a Hartmann number $M=1000$.*

The pressure gradient calculated by equation *(2.2l)* reads

$$\partial_x p = \frac{(\partial_x p)_H}{1 - (\partial_x p)_H \frac{\epsilon}{c_S b}} . \qquad (2.4k)$$

ϵ is given by $\epsilon = \Sigma 2/\beta_i^4 = 1/3$ and $(\partial_x p)_H = -(c+1/M)/(c+1)/(1-1/M)$ is the pressure gradient in Hartmann flow $(b \rightarrow \infty)$.

Figure 2.4 shows some velocity profiles of well known MHD-flows in a square channel for different values of the side wall conductance ratio c_S. The conductivity of the Hartmann walls is $c = 0.1$ and the Hartmann number is $M = 1000$. For any conductivity of the side walls the flow in the whole core shows a uniform velocity profile with thin boundary layers at Hartmann walls. For highly conducting side walls the flow shows only weakly higher velocities near the side walls, but still the overall character of the flow is of slug flow type. If c_S is decreased the core is still of slug type. In the side layers, however, high velocity jets appear which can carry a significant amount of the total volume flux. The reason for this velocity overshoot is a kind of electromagnetic pumping in the side layers. The energy is taken form the core which acts as a generator.

It is obvious that velocity distributions as shown in figure 2.4 should have significant influence on heat and mass transfer conditions at channel walls. The thickness of the Hartmann layers, which is of the order M^{-1} is for fusion applications $(M = 10^4 \div 10^5)$ in general much thinner than convective- diffusive boundary layers. The transport of heat and mass near the Hartmann walls is therefore expected to be equivalent to that in theoretical slug flow. The high velocity jets in the side layers $(u = O(M^{\frac{1}{2}}))$, however, should lead to improved transfer compared to flow of slug type. If the conductivity of all walls is very poor (i.e. $c = c_S << M^{-\frac{1}{2}}$) equation *(2.4a)* does not hold. It can be shown by detailed analysis (see for example Moreau 1990 page 141) that for such conditions the overshoot in the side layer velocities disappears. Transfer conditions for heat and mass at the side walls are reduced at least to those in slug flow.

3 Convective– diffusive Transport

3.1 Transport Equations

Stationary convective– diffusive transport of scalar properties like heat or the mass of dissolvable components may be described by the equation for non-dimensional temperature $T=(T^*-T_0^*)/\Delta T^*$ ('*' denotes here the physical property, the index '$_0$' stands for reference case)

$$Pe_T(\boldsymbol{v}\cdot\nabla)T = \nabla^2 T + \dot{q} \qquad (3.1a)$$

or for the scaled mass concentration $C=(C^*-C_0^*)/\Delta C^*$ of a solute

$$Pe_C(\boldsymbol{v}\cdot\nabla)C = \nabla^2 C + S\ . \qquad (3.1b)$$

ΔT^* and ΔC^* are characteristic scales for temperature and mass concentration.

The thermal and solutal diffusivities κ and D are assumed to be constant. They are used to form the ***Peclet numbers*** $Pe_T=v_0L/\kappa$ and $Pe_C=v_0L/D$, respectively.

The source term $\dot{q}$ describes the effect of volumetric heating due to dissipation, Joule's heating by electric currents, nuclear radiation, or chemical reaction.

S represents source or sink terms for the mass of a solved species, arising for example from chemical reaction.

For fully developed flows equation *3.1a* and *3.1b* can be written as

$$u\partial_\xi T = \nabla^2 T + \dot{q}\ , \qquad (3.1c)$$

$$u\partial_\xi C = \nabla^2 C + S\ , \qquad (3.1d)$$

where ξ is the axial coordinate scaled not only by the characteristic dimension L of the cross section, but in addition by the Peclet numbers Pe_T and Pe_C, respectively. This normalization accounts for the difference in characteristic time scales for diffusion $\tau_\kappa=L^2/\kappa$ and for convection $\tau_u=L/u$. In the same time as a property is transported in the cross section by diffusion over a length L this property is transported by advection in the x-direction over a distance $X=L\cdot Pe$. This scales provide the basis for a unique solution of the general transport problem for all Peclet numbers. For $\xi>>1$ the heat and mass transfer is fully developed, whereas for $\xi<<1$ the solution of *3.1c* or *3.1d* is of

boundary layer type.

3.2 Boundary conditions

As thermal boundary condition at thin walls of thickness t the temperature T_w at the outer wall surface is related to the temperature T at the fluid-wall interface and to the normal gradient component of the fluid temperature at the wall by the equation

$$Bi(T-T_w) + \partial_n T = 0 \; . \qquad (3.2a)$$

The ***Biot number*** $Bi=\lambda_w L/\lambda t$ describes the relative thermal conductivity of the wall in the normal direction. λ_w/λ is the ratio of thermal conductivity of the wall and the fluid.

If $Bi \rightarrow \infty$ the wall is a perfect heat conductor and the fluid temperature at the wall becomes equal to the given temperature outside. If $Bi \rightarrow 0$ the wall is thermally insulated.

For a given surface heat flux q the thermal boundary condition reads

$$q = -\partial_n T \; . \qquad (3.2b)$$

There are several relevant temperature scales depending on the considered problem. The scales are $\Delta T^*=T_w^*{}_{max}-T^*_{min}$, $\Delta T^*=q^*_{max}L/\lambda$, or $\Delta T^*=q^*_{max}L^2/\lambda$, if either the distribution of wall temperature, of surface heat flux, or volumetric heating is the mainly determining mechanism of heat input.

As solutal boundary condition it is supposed that for corrosion or deposition processes at channel walls the transferred mass flux s^* is proportional to the under or super saturation to some power m.

$$s^* = K(C^*-C_e^*)^m \; . \qquad (3.3a)$$

C_e^* denotes the saturation concentration which may depend strongly on the actual temperature T^*. Since the mass flux has to equal the diffusive flux at the wall the final non-dimensional condition reads

$$(C-C_e)^m + \frac{1}{Da}\,\partial_n C = 0 \; , \qquad (3.3b)$$

with the **Damköhler number** $Da=\Delta C^{*m-1}KL/D$. Da represents the ratio of diffusion time $\tau_D=L^2/D$ and a characteristic time scale for chemical surface reaction $\tau_K=L/K\Delta C^{m-1}$ (Brauer 1971, p.439). The mass transfer from the fluid to the wall (or opposite) is limited by diffusion if $Da\longrightarrow\infty$ or by surface reaction as $Da\longrightarrow 0$.

3.3 Numerical solution

Equations *3.1c* or *3.1d* permit tractable analytical solutions only for special cases of the boundary conditions (see for example Gardner 1967, who calculates heat transfer in fully developed MHD pipe flow with constant wall heat flux). Numerical methods lead to fast and accurate results with acceptable effort in the case when entrance effects at the inlet to a heated section or non-uniform wall temperature or wall heat flux have to be taken into account. Therefore a numerical approach is used to solve the general transport equation. Analytical results are used to verify the used numerical scheme.

The equation *3.1c* can be replaced by the more general equation

$$U\partial_\xi T = A_\eta\partial_{\eta\eta}T + B_\eta\partial_\eta T + A_\zeta\partial_{\zeta\zeta}T + B_\zeta\partial_\zeta T + CT + D \qquad (3.4a)$$

with boundary conditions

$$u\partial_\xi T = b_\eta\partial_\eta T + cT + d \quad at \quad \eta = \eta_{min} \text{ and } \eta_{max} \qquad (3.4b)$$

and

$$u\partial_\xi T = b_\zeta\partial_\zeta T + cT + d \quad at \quad \zeta = \zeta_{min} \text{ and } \zeta_{max} \qquad (3.4c)$$

which may be used to describe convective– diffusive heat transport in any locally orthogonal $x\eta\zeta$-coordinate system. All coefficients in equations *3.4a-c* are arbitrary functions. Equation *3.4a* approximates the transport equation *3.1c* only if the diffusive axial heat flux $\partial_\xi T$ is negligible compared with the convective one uT. This is approximately the case for high Peclet numbers or for extremely long channels compared to the characteristic cross section dimension.

With the coordinates $\eta=y$, $\zeta=z$ and the coefficients

$$\begin{aligned} A_y &= 1 , \quad B_y = 0 , \\ A_z &= 1 , \quad B_z = 0 , \\ C &= 0 , \quad D = q , \end{aligned} \tag{3.5a}$$

the equation *3.4a* describes suitably the transport in rectangular geometries.

For $\eta=r$, $\zeta=\varphi$ and

$$\begin{aligned} A_r &= 1 , \quad B_r = \frac{1}{r} , \\ A_\varphi &= \frac{1}{r^2} , \quad B_\varphi = 0 , \\ C &= 0 , \quad D = q , \end{aligned} \tag{3.5b}$$

the transport in a circular pipe can be easily modeled.

Equation *3.4a* also permits calculations with higher resolution near the channel walls if other types of non-linearly stretched coordinates are introduced. This may be useful for calculations with very high values of *Pe* ($\xi << 1$), when the temperature or concentration show extremely thin boundary layers.

The equidistant grid used for numerical calculations is shown in figure 3.1. Values of unknown scalar properties are placed in the center of each corresponding control volume. An *ADI* scheme is used for integration in the ξ-direction to ensure numerical stability of the solution and to avoid restrictions on the step width $\Delta\xi$. The discrete approximation of equation *3.4* reads for one step

$$U \frac{T^{\xi+}_{\eta,\zeta} - T^{\xi}_{\eta,\zeta}}{\Delta\xi} = \tag{3.6a}$$

$$A_\eta \frac{T^{\xi+}_{\eta+,\zeta} - 2T^{\xi+}_{\eta,\zeta} + T^{\xi+}_{\eta-,\zeta}}{\Delta\eta^2} + B_\eta \frac{T^{\xi+}_{\eta+,\zeta} - T^{\xi+}_{\eta-,\zeta}}{2\Delta\eta} + \tag{3.6b}$$

$$A_\zeta \frac{T^{\xi}_{\eta,\zeta+} - 2T^{\xi}_{\eta,\zeta} + T^{\xi}_{\eta,\zeta-}}{\Delta\zeta^2} + B_\zeta \frac{T^{\xi}_{\eta,\zeta+} - T^{\xi}_{\eta,\zeta-}}{2\Delta\zeta} + \tag{3.6c}$$

$$C \frac{T^{\xi+}_{\eta,\zeta} + T^{\xi}_{\eta,\zeta}}{2} + D \tag{3.6d}$$

The upper indices ξ or $\xi+$ denotes the position ξ or $\xi+\Delta\xi$ in axial direction, respectively. The lower indices specify the coordinates in the cross section. For example $T^{\xi}_{\eta,\zeta+} = T(\xi,\eta,\zeta+\Delta\zeta)$. In the proceeding next step the upper index $\xi+$ in term *(3.6b)*, representing the implicit part of the scheme, is changed in ξ, describing an explicit term, and vice versa in term *(3.6c)*.

The value of the unknown function T at the boundary is not defined by the discrete grid. In the equations for the general boundary conditions this value is estimated as an average value of the fictive and the first physical value lying half a grid spacing outside and inside the computational domain. The normal derivative is estimated directly at the border as a central difference between fictive and physical values.

The above described procedure for calculating the fluid temperature may also be used for determining the concentration field of a solved component if T is replaced by C. The boundary condition for higher order reactions $(m>1)$ *3.3b* needs some modifications. For this reason the reaction term is expanded into Taylor series.

$$(C-C_e)^m = (C-C_e)^m\big|_{\xi} + m(C-C_e)^{m-1}\big|_{\xi}\partial_{\xi}(C-C_e)\Delta\xi \ . \qquad (3.6e)$$

This leads finally to the boundary condition

$$\frac{1}{m}(C-C_e)\big|_{\xi} + \Delta\xi\partial_{\xi}(C-C_e) + \frac{1}{m(C-C_e)^{m-1}\big|_{\xi}}\frac{1}{Da}\partial_n C = 0 \ , \qquad (3.6f)$$

which is covered by the general formulation *3.4b* and *3.4c*.

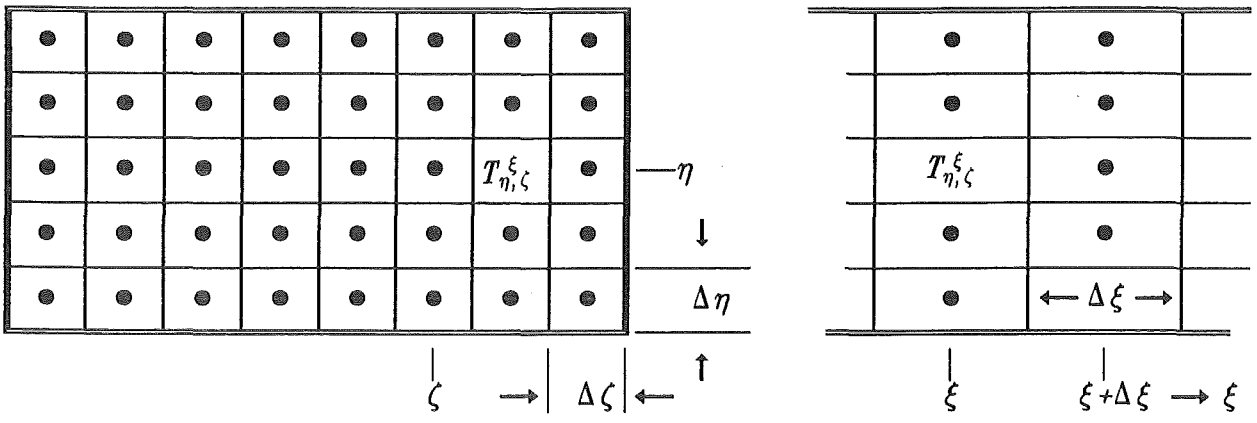

Figure 3.1 Numerical grid.

4 Heat transfer conditions in circular pipes

The most important duct geometry for technical applications is the circular pipe. The discussion of heat transfer in MHD duct flow is started with fully developed conditions for different surface heat fluxes. The first one is the constant wall-normal heat flux $q=-e_r$. The second one is the more relevant case for applications in poloidal fusion blankets with a constant planar heat flux from the plasma towards the wall, $q=-e_z$. Three-dimensional solutions for the second type of heat flux are considered at the entrance of the cold fluid to a heated section.

4.1 Fully developed heat transfer into a circular pipe at constant heat flux $(q=-e_r)$

At first, results for fully developed heat transfer into circular pipes $(\xi>>1)$ are discussed. The flow distribution $u(r,\varphi)$ is obtained from the asymptotic result *(2.2h* and *2.3b)*. The heat flux q^* at the channel wall is assumed to be constant and used for temperature scale $\Delta T^*=q^*L/\lambda$. Analytical solutions to this problems for a wide range of the Hartmann number have been obtained by Gardner 1967. In the following chapter his results are compared with numerically obtained results for code verification.

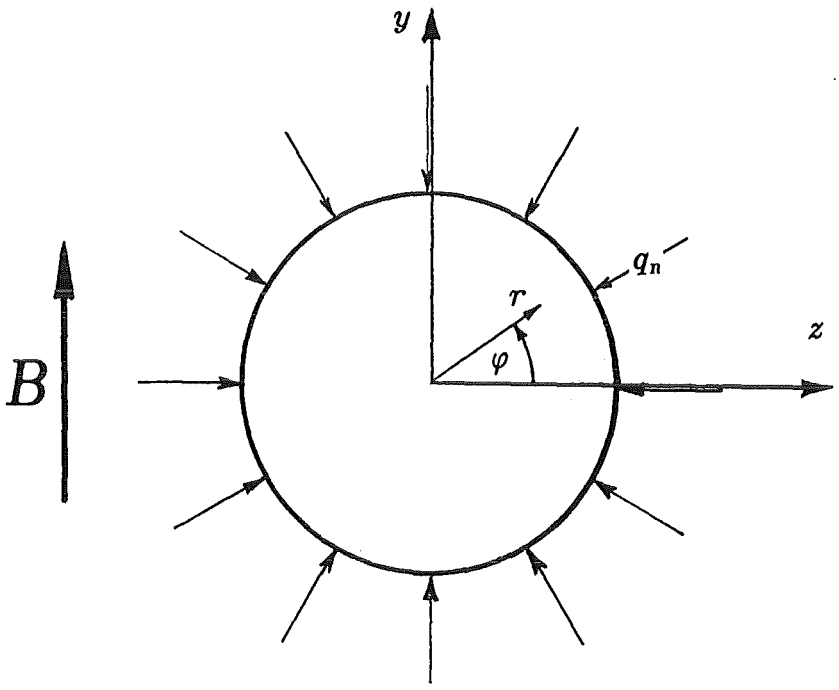

Figure 4.1 Constant wall-normal heat flux $q=-e_r$ into a circular pipe

The fully developed axial temperature gradient is independent of the flow structure and given by

$$\partial_\xi T = \partial_\xi T_m = 2, \qquad (4.1)$$

where the T_m is the bulk mixing-cup temperature defined as the average convective heat flux over the cross section A.

$$T_m(\xi) = \frac{1}{A}\int_A u \cdot T dA. \qquad (4.2)$$

The ***Nusselt number***

$$Nu = \frac{2}{T_w - T_m} \qquad (4.3)$$

characterizes the heat transfer conditions at the channel walls and is a direct measure for the temperature gradient at the wall in terms of the mean temperature T_m and the local wall temperature T_w. For special velocity profiles like the bulk flow $u=1$ or the hydrodynamic case $u=2(1-r^2)$ the Nusselt number is given analytically as $Nu=8$ and $Nu=48/11$, respectively. These values are used to check the accuracy of the numerical method. Figure 4.2a and 4.2b show the relative deviations of the numerically obtained solutions from the exact ones for different numbers of grid points n_r and n_φ. The relative numerical error is reduced by two decades if the grid size is reduced by one. This reflects the second order accuracy of the used numerical scheme. The fast convergence towards the analytical solution for the Nusselt number ensures that the equation has been implemented correctly in the directions of η (here r) and ζ (here φ). A check for the axial temperature gradient ensures correct discretization in the ξ-direction.

Gardner presents solutions for the Nusselt number at the duct wall of an electrically insulating pipe in a magnetic field. In a strong field the velocity profile is not axisymmetric. The velocity gradient at the channel wall depends strongly on the angle φ, which results in variable heat transfer conditions along the duct's perimeter. A comparison of $Nu(\varphi)$ (results obtained by Gardner, see figure 4.3a) with the numerical solution for $M=100$ and $M=1000$ (figure 4.3b) is shown in figure 4.3. The numerical solution, in which the asymptotic velocity profile $(2.3b)$ is used shows good agreement with Gardner's analytical results. For lower values of the Hartmann number the asymptotic

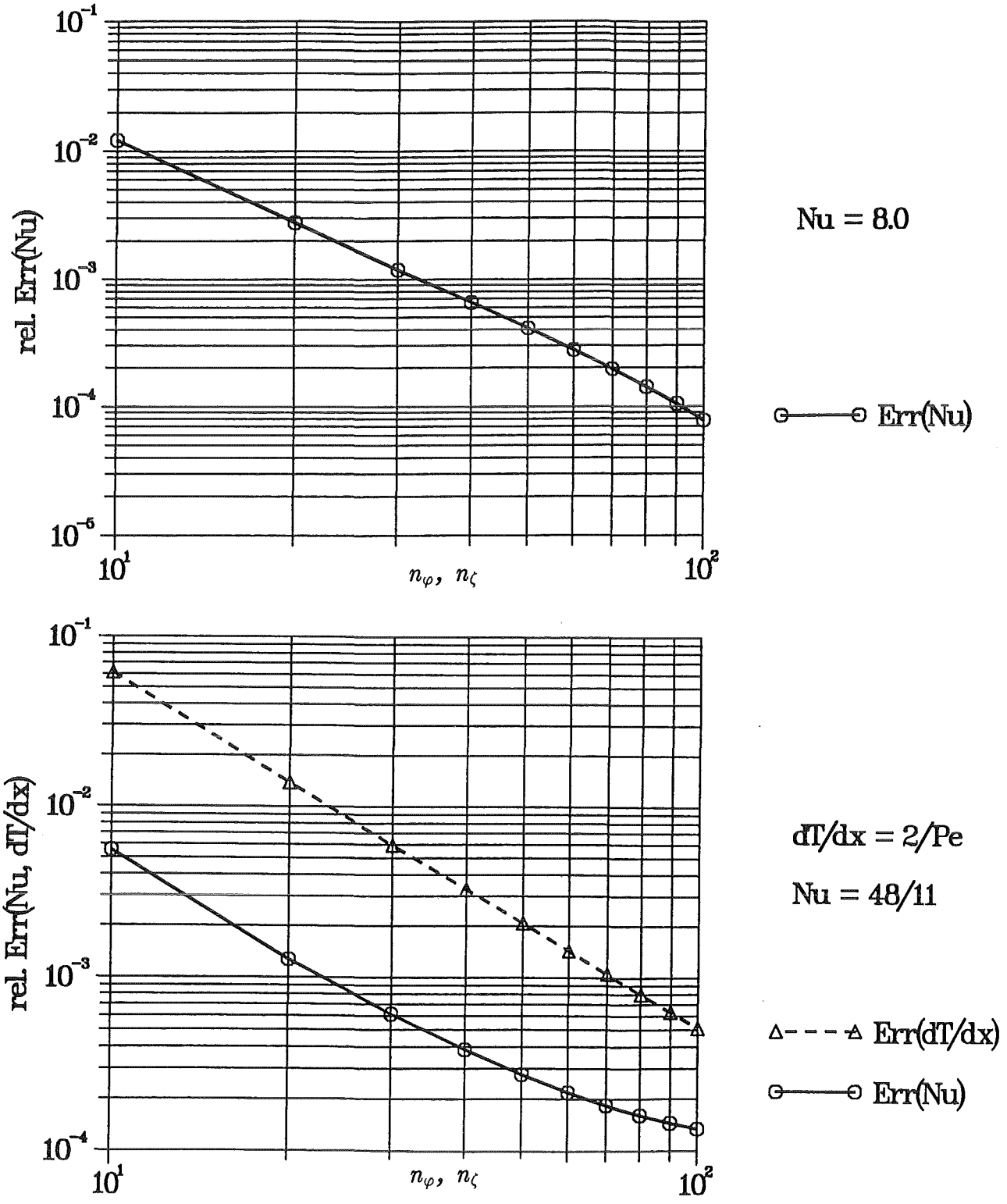

Figure 4.2 Check of convergence of the numerical scheme

approach does not lead to an accurate solution for velocity near $\varphi=90°$, since the Hartmann layer assumption, that viscous layers are much thinner than the core dimension, fails to account for viscous effect properly.

For a given wall heat flux the property of primer interest is the wall temperature. It should not exceed a certain value, which is limited by the wall material. High temperature gradients in the structure may cause unacceptable material stress. For these reasons the Nusselt number as characteristic measure for heat transfer is dropped and further discussions of results are restricted to the wall temperature T_w.

The results obtained by Gardner are valid for MHD flows in insulating pipes only. However, for fusion applications also pipes with thin electrically conducting walls are considered. Results for fully developed heat transfer conditions with constant radial heat flux $q_n=-1$ are shown in figure 4.4 for a high Hartmann number $M=1000$ and a variety of wall conductance ratios $(c=0 \div 1)$. For high values of c $(c>>M^{-1})$ the flow is of slug type. The difference between the local wall temperature $T_w(\varphi)$ and T_m does almost not depend on the circumferential coordinate φ. The value of $T_w-T_m=0.25$ corresponds directly to the Nusselt number $Nu=8$ of a bulk flow. For the fusion relevant value $c=0.01$ most of the flow is still carried by a core with constant velocity (remember the velocity distribution in figure 2.2b). Only in very narrow regions near $\varphi=0$ or $\varphi=\pi$ there is a small reduction of velocity. The influence of this decreased velocity on heat transfer gives a distinct variation of the wall temperature $T_w(\varphi)$. The largest variations in wall temperature are found for electrically insulating pipes with values of $\Delta T_{w,max}=0.13$.

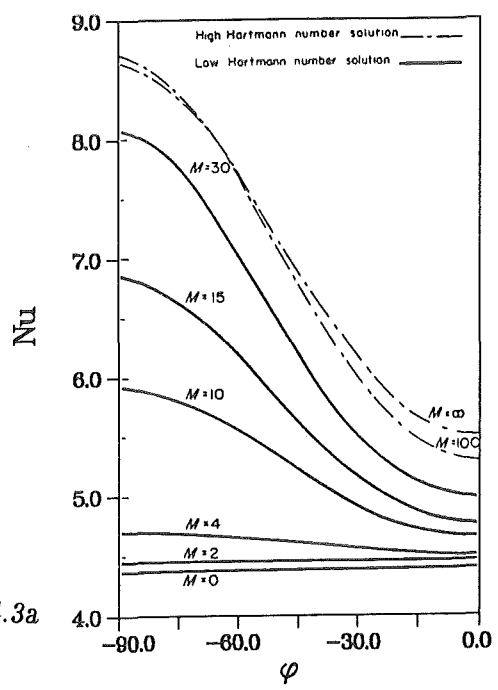

fig 4.3a

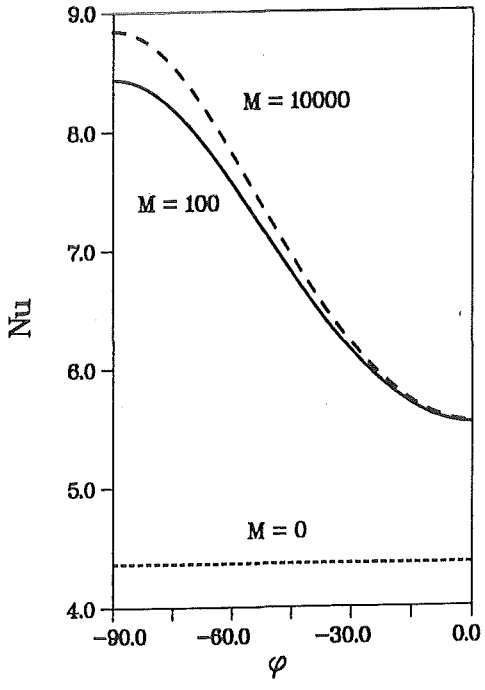

fig. 4.3b

Figure 4.3 *Comparison of analytically (fig 4.3a Gardner 1967) and numerically (fig. 4.3b) obtained results for Nu for fully developed heat transfer conditions.*

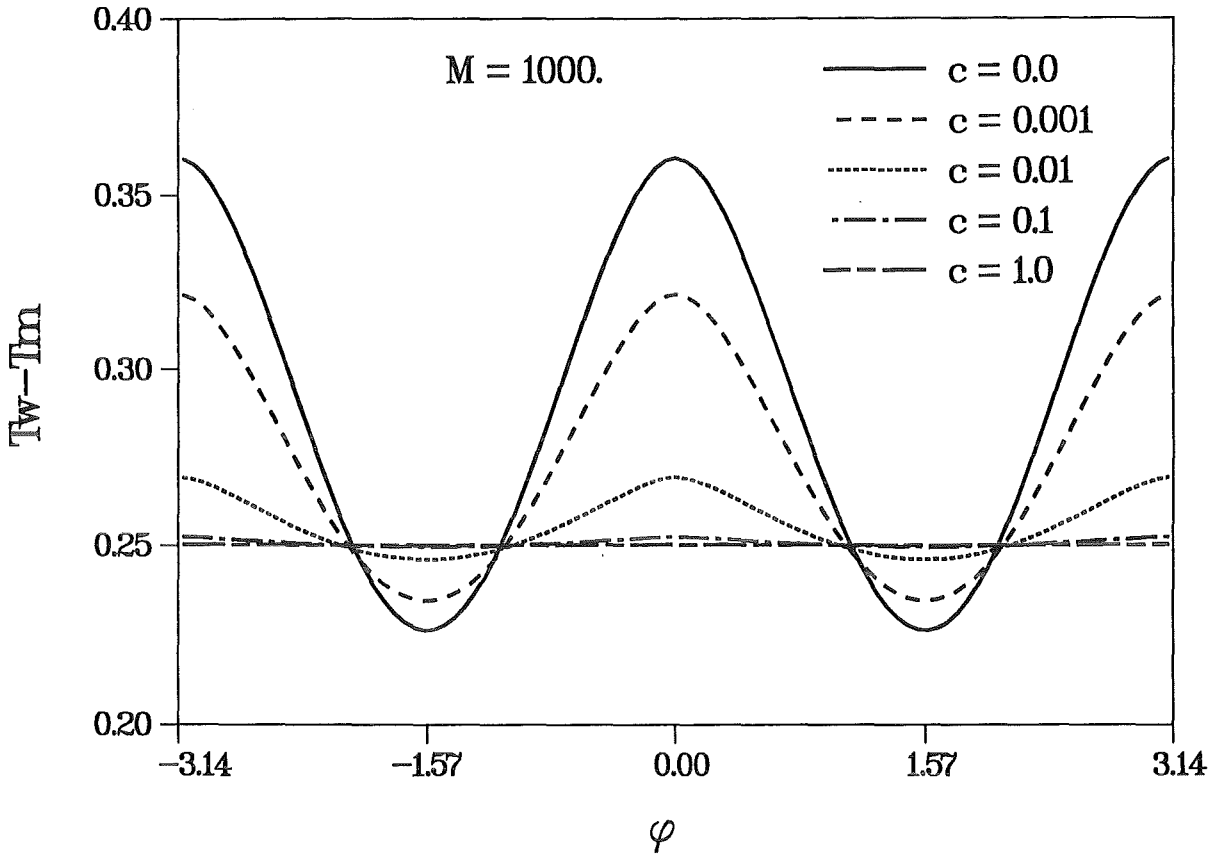

Figure 4.4 *Difference between wall temperature and mean temperature of an MHD flow in a circular pipe heated by constant wall-normal heat flux. The thermal conditions are fully developed; M=1000.*

4.2 Fully developed heat transfer into a circular pipe at constant heat flux ($q=-e_z$)

For fusion applications a more relevant case is the cooling pipe, which is exposed not to a rotationally symmetric thermal radiation field $n \cdot q(\varphi)=q_n=const.$ as described before, but, to a planar radiative heat flux $q=-e_z$. The wall normal component is determined as $q_n=-\cos\varphi$ for the part of the wall which faces the plasma $(-\frac{1}{2}\pi<\varphi<\frac{1}{2}\pi)$ and $q_n=0$ for the rest (see figure 4.6a).

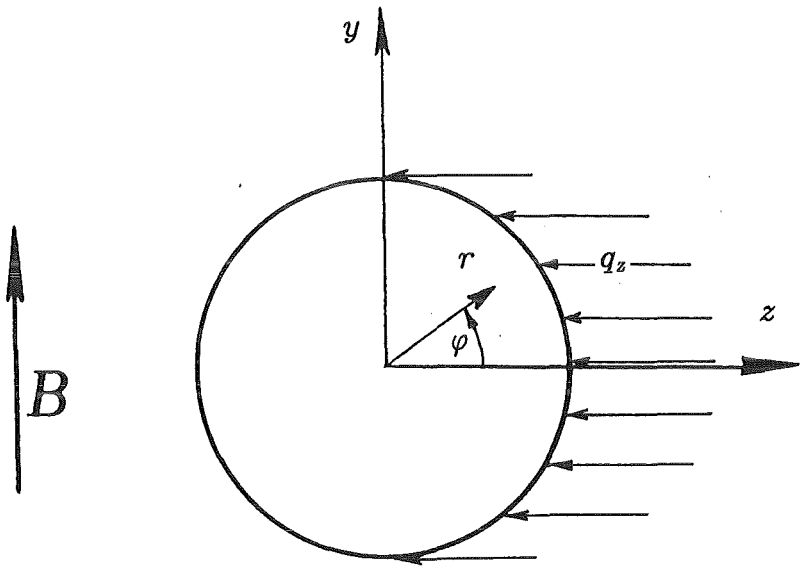

Figure 4.5 Constant planar heat flux $\boldsymbol{q}=-\boldsymbol{e}_z$ into a circular pipe

The change in convective transport with axial length is determined by the heat input over the channel wall. The fully developed axial temperature gradient for a heat flux $q(\varphi)$ is given by

$$\partial_\xi T_m = \frac{1}{A}\int q_n db \ , \qquad (4.4)$$

where $\int q_n db$ is the integrated normal heat flux along the border of the cross section A. For the special heat flux considered in this chapter the axial temperature gradient is

$$\partial_\xi T_m = \frac{2}{\pi} \ . \qquad (4.5)$$

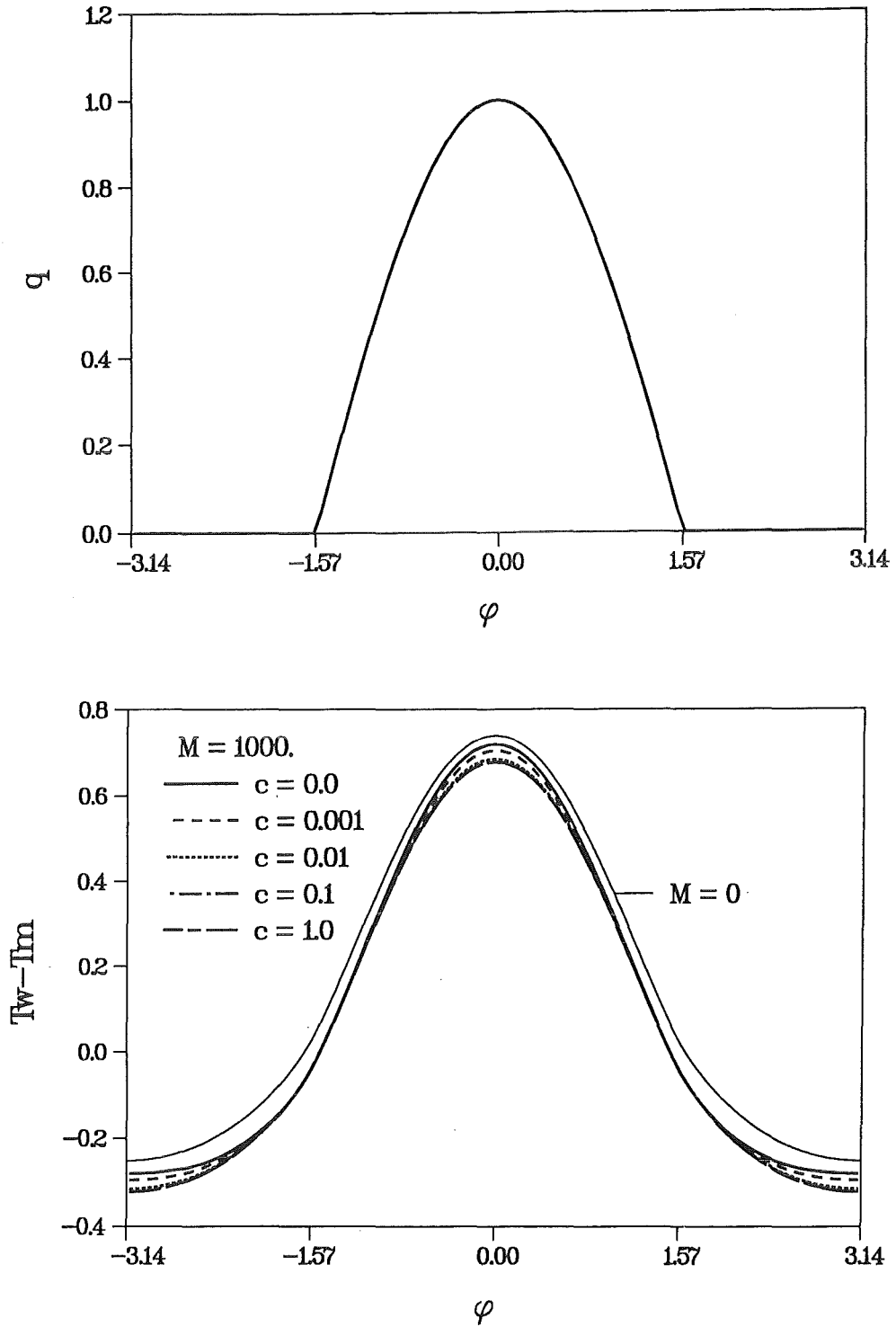

Figure 4.6 *Difference between wall temperature and mean temperature of an MHD flow in a circular pipe heated by constant planar heat flux. The thermal conditions are fully developed; M=0 and M=1000.*

Calculated wall temperatures for a hydrodynamic case $(M=0)$ and for fusion relevant MHD flows (magnetic field is perpendicular to the direction of heat flux $\varphi=0$, $M=1000$, $c=0 \div 1$) are shown in figure 4.6b. The non-symmetric heating due to the planar heat flux leads to much higher temperature differences in the cross section compared to the case with constant wall heat flux, even if the total heat input per unit length is smaller by a factor of $1/\pi$. $\Delta T_{w,max} \sim 1$ for all considered flow types. It is interesting to notice that the influence of the magnetic field on heat transfer conditions is very poor. It leads only to a shift in the temperature range of about -0.07. The MHD - heat transfer conditions in insulating pipes are very close to those in hydrodynamic flows because the velocity profile shows similar distribution in the direction of the main heat flux compared to the hydrodynamic case. However, even a slug flow velocity profile which is achieved for electrically well conducting walls $(c>>M^{-1})$ at high Hartmann numbers can not improve the equalization of the cross sectional wall temperature.

To complete these considerations the magnetic field is turned by 90^{o} in exactly the direction of the heat flux. For such conditions the high velocity gradients of MHD flows in electrically insulating channels coincide with positions where the heat flux is highest. The heat transfer is comparable to bulk flow conditions. The highest wall temperature is reduced by $\Delta T=0.068$ (see figure 4.7).

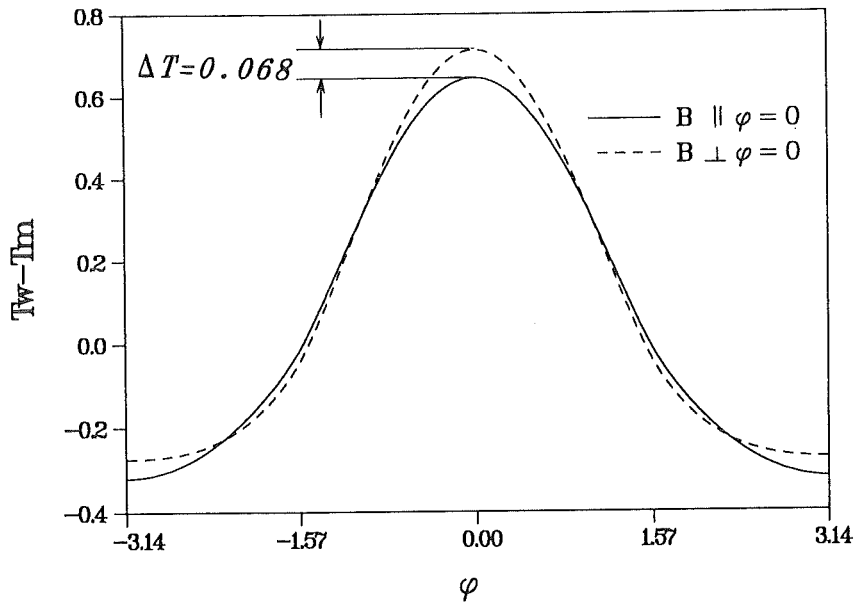

Figure 4.7 Difference between wall temperature and mean temperature of an MHD flow in an electrically insulated circular pipe. The thermal conditions are fully developed; $M=1000$. The constant thermal heat flux is either aligned with the magnetic field ($B \parallel \varphi=0$) or perpendicular to it ($B \perp \varphi=0$).

4.3 Three-dimensional effects at the entrance of a heated section

In the previous paragraphs the fully developed heat transfer conditions in circular pipe flow have been discussed in detail. In technical applications, however, fully developed conditions are reached after some developing length behind the entrance of a heated section.

Figure 4.8 shows the transition of some interesting properties form entrance conditions to fully developed conditions as a function of the axial coordinate ξ for a hydrodynamic flow with constant heat input $q_n=-1$ at the channel wall. It shows the mean temperature T_m, the wall temperature T_w and the difference T_w-T_m. Fully developed conditions as described before $(\partial_\xi T_w=2,\ T_w-T_m=11/24)$ are almost reached at $\xi=0.3$.

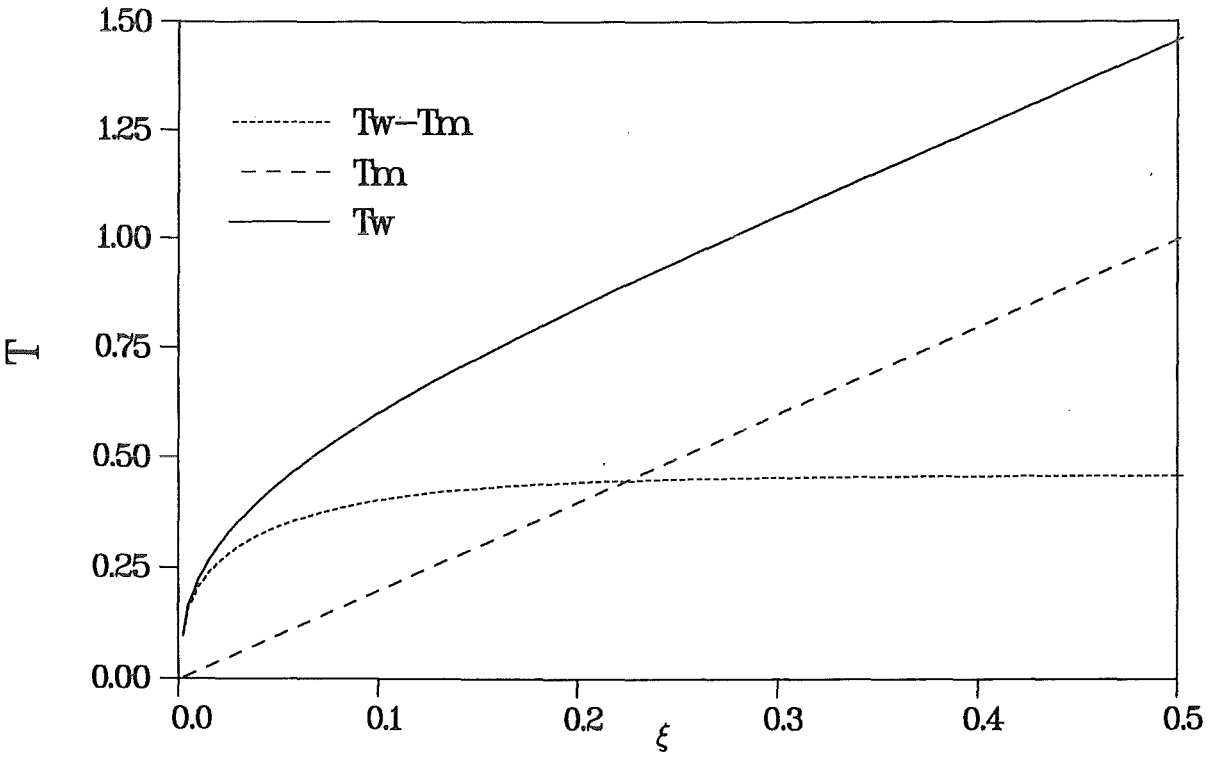

Figure 4.8 *Wall– and mean temperature and their difference, developing with axial length ξ. The wall-normal heat flux is constant; $M=0$.*

For a blanket relevant heat flux $q_n=-\cos\varphi$ and MHD flow in an electrically insulating pipe $(M=1000,\ B\perp q)$ the developing length is approximately three times longer. This can be seen from figure 4.9. Fully developed heat transfer $(\partial_\xi T_w=2/\pi)$ is reached at $\xi=1$. For real applications the Peclet number can be much larger than the total channel length x_{max} $(\xi<<1)$ so that heat transfer in the whole blanket element happens within the transition zone. The heat transfer is of boundary layer type along the heated part of the wall for very small values of ξ (see figure 4.10). This thermal boundary layer grows continuously towards the duct center with increasing ξ. At $\xi=0.1$ the half of the duct is affected by the thermal disturbance. If $\xi=1$ fully developed conditions are approximately reached. The isotherms become almost straight equally spaced lines near $z=1$, corresponding to the constant heat flux $q=-e_z$.

The most important question for fusion blanket applications is, weather the maximum wall temperature at the end of a heated section is within acceptable limits, or in other words, what Peclet number is necessary to ensure wall temperatures below the limit. If the highest tolerable wall temperature $T_{w,max}$ is known the relation shown in figure 4.9 can be used to determine ξ_{max} and finally the required Peclet number $Pe_{rec}>x_{max}/\xi_{max}$. Pe_{req} determines the characteristic velocity and MHD pressure drop.

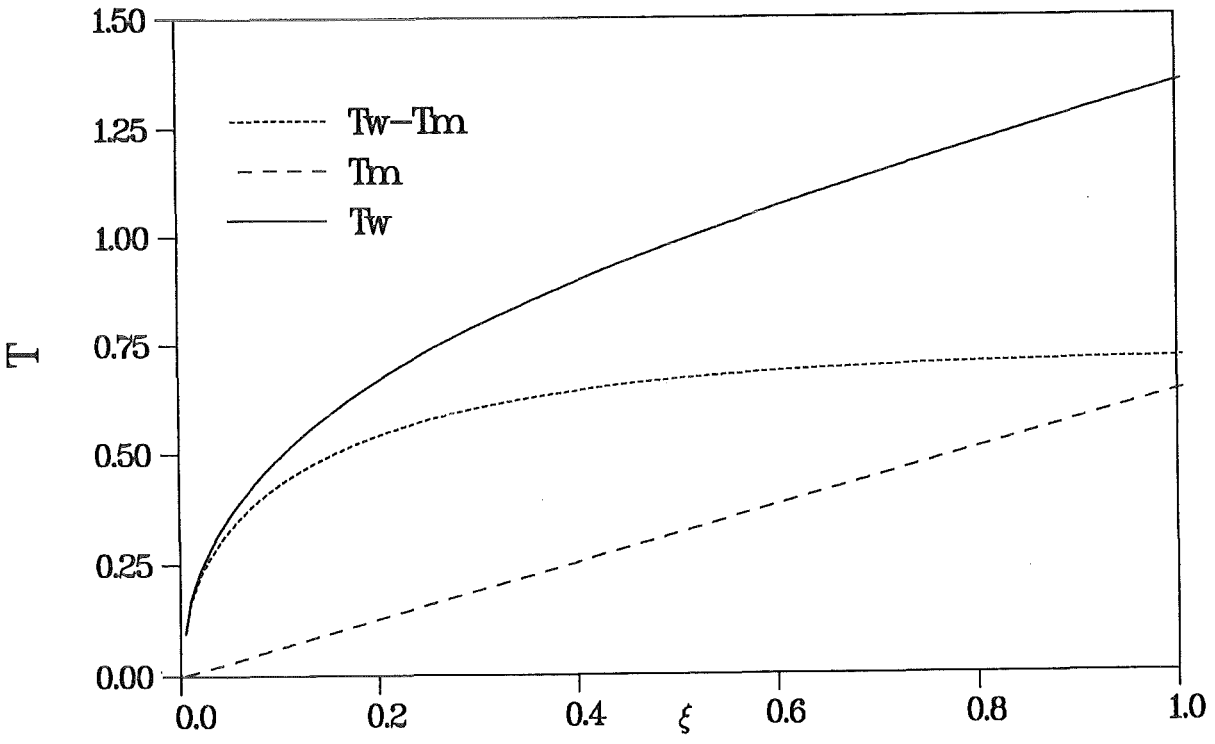

Figure 4.9 *Highest wall– and mean temperature and their difference, developing with axial length ξ. The heat flux is planar and constant; $M=1000$.*

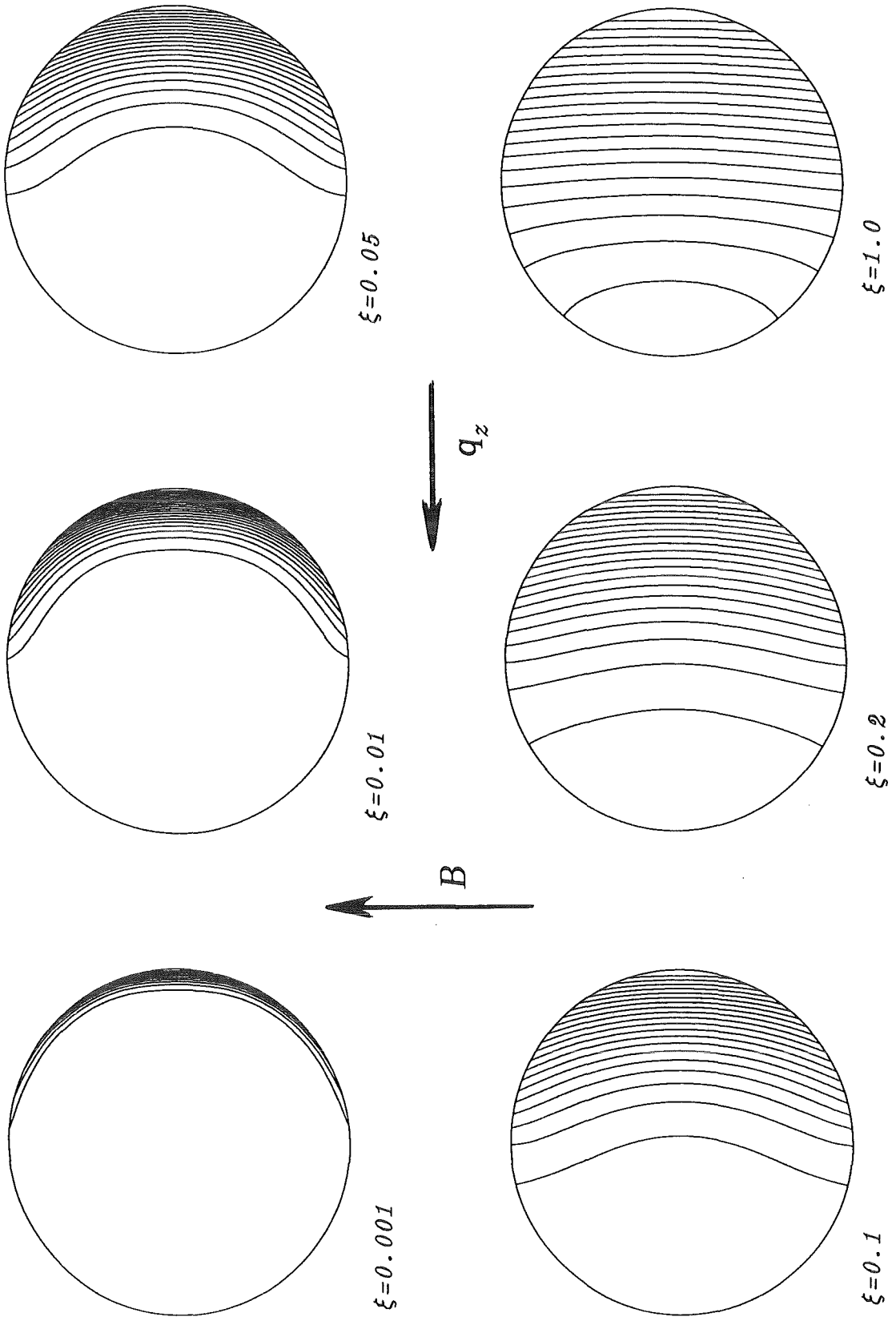

Figure 4.10 *Development of thermal boundary layers in a circular pipe. The heat flux is planar and constant; M=1000, c=0.*

5 Heat transfer conditions in rectangular ducts

The other widely used duct geometry for technical applications is the duct with rectangular cross section. As in the previous paragraph fully developed conditions are discussed first for two different cases of heat flux. The first one is the constant wall-normal heat flux $q_n=-1$. The effect of a constant planar heat flux $\boldsymbol{q}=-\boldsymbol{e}_z$ entering the cooling duct of a poloidal fusion blanket is discussed for fully developed and three-dimensional heat transfer conditions.

5.1 Fully developed heat transfer into a rectangular duct at constant heat flux ($q_n=-1$)

MHD flows in rectangular ducts have been described in paragraph 2.4. The steep velocity gradients at channel walls should lead to favorable heat transfer. Thin jets along the side walls exist for several combinations of the wall conductance ratios c and c_S of the Hartmann walls and side walls. They can carry a significant amount of the total flow rate. These jets exhibit very high velocities compared to that in the flat core, which occupies the rest of the cross section (remember the velocity profiles shown in figure 2.3).

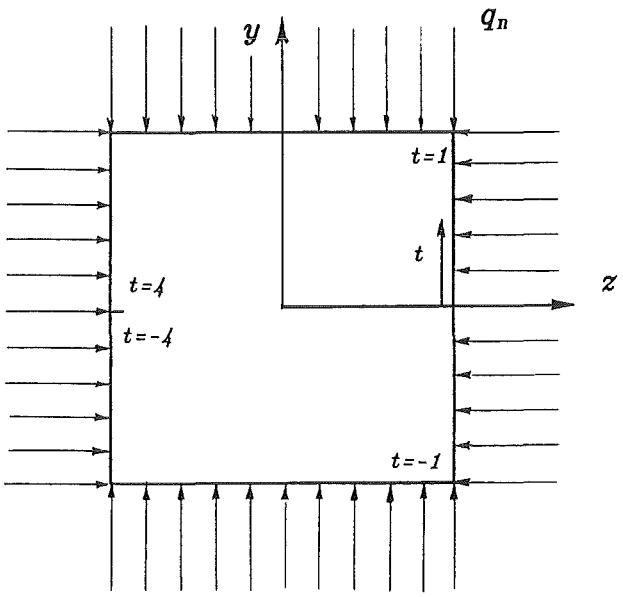

Figure 5.1 Constant wall-normal heat flux $q_n=-1$ into a square duct

Consider a rectangular duct exposed to a constant wall-normal heat flux $q_n=-1$. The effect of such heating on wall temperature for fully established conditions is shown in figure 5.2 for several characteristic MHD velocity profiles. This figure shows the variation of the wall temperature along a wall-tangential coordinate as indicated in figure 5.1 for different ratios c_S/c. Even if the flow is of slug type (this is the case for $c_S/c>>1$) there are large variations in the wall temperature $\Delta T_{w,max}=0.49$. Heat transfer at Hartmann walls and side walls is approximately the same. Differences would be only possible if the solution for temperature would be of boundary layer type with a thermal layer much thicker than the Hartmann layer $\delta_T>>\delta_H \sim M^{-1}$ but much thinner than the side layer $\delta_T<<\delta_S \sim M^{-\frac{1}{2}}$. However, in a fully developed thermal field this is never the case. The large variations of T_w can be explained by the heat input to a fluid

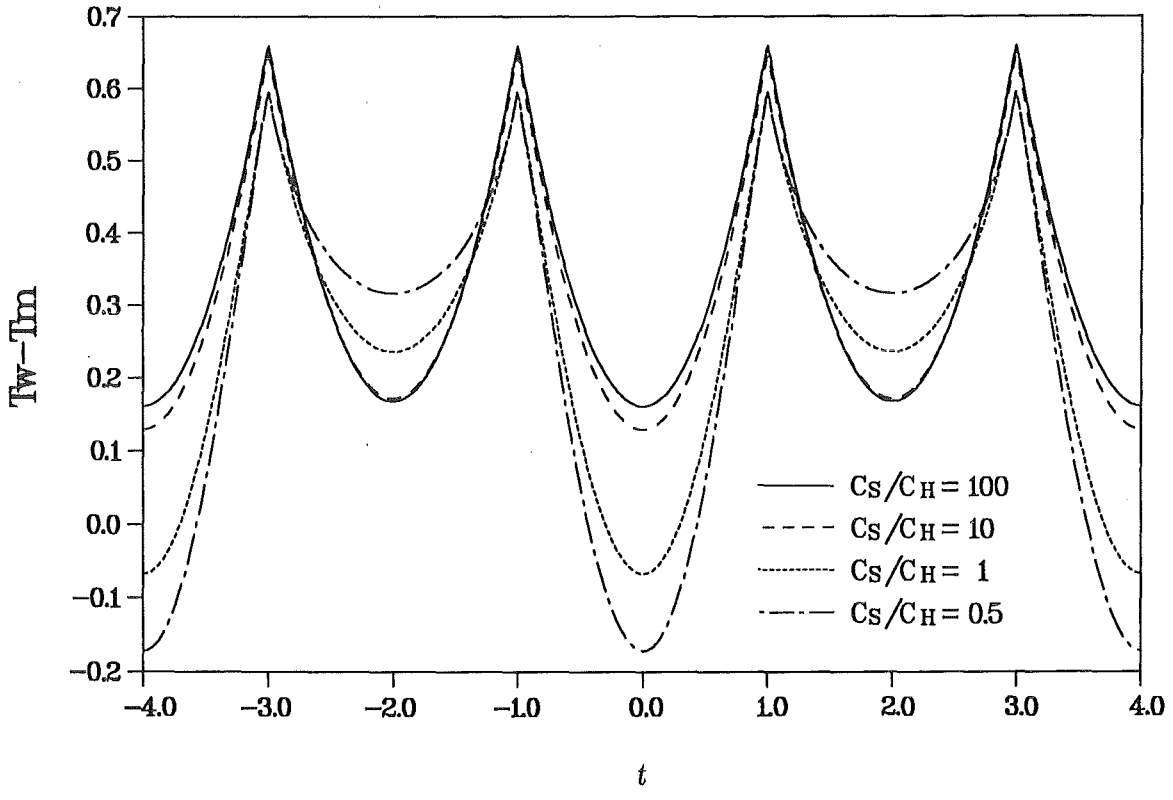

Figure 5.2 *Difference between wall temperature and mean temperature of an MHD flow in a square duct heated by constant wall-normal heat flux. The thermal conditions are fully developed; $M=1000$.*

lement at the corners. This heat input happens from two sides simultaneously whereas the diffusive transfer into the bulk of the flow is restricted to one direction only (the 'radial' one) with exchange area much smaller than the area of heating at the walls. Near the center of each Hartmann or side wall this unpleasant heat transfer situation does not exist and wall temperatures are moderate. The situation at the side wall may be improved further for the jet flow, when $c_S/c<<1$. An increase in the jet flow rate leads to a decrease in the core velocity and consequently to higher wall temperatures at the Hartmann walls. For a ratio $c_S/c=0.5$ the maximal temperature difference in the cross section is about $\Delta T_{w,max}=0.77$.

5.2 Fully developed heat transfer into a rectangular duct by constant heat flux $(q=-e_z)$

For a fusion typical heat flux $q=-e_z$ at the plasma facing side wall of a rectangular poloidal cooling channel the distribution of wall temperature becomes similar to those in a circular duct exposed to the same heat flux. The maximal difference in wall temperature $\Delta T_{w,max}=0.97$ is higher, even if the total heat input is only one quarter of that discussed in the previous case where all walls have been heated (see figure 5.4). The influence of the velocity profile on heat transfer is only minor. There is no significant qualitative change in wall temperature if there is a high velocity jet at the heated side or not. The main effect is a total shift -0.11 in wall temperature to lower values if c_S/c varies from 100 to 0.5. The temperatures at the heated side wall and (surprisingly also) at the adiabatic side wall are slightly deformed. The expected enormous improvement in heat transfer by the high velocity jets near a heated side wall can not be found in a laminar thermally fully developed problem.

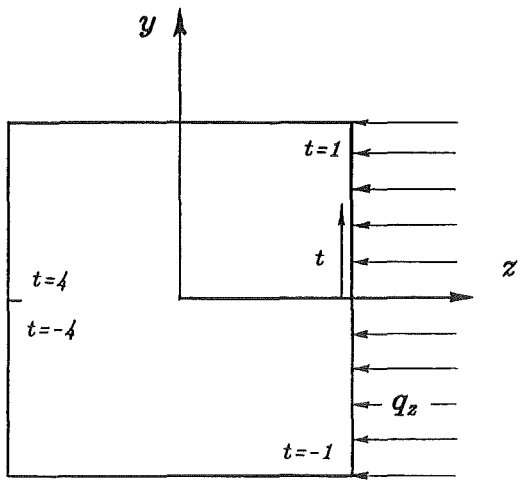

Figure 5.3 Constant planar heat flux $q_n=-e_z$ into a square duct

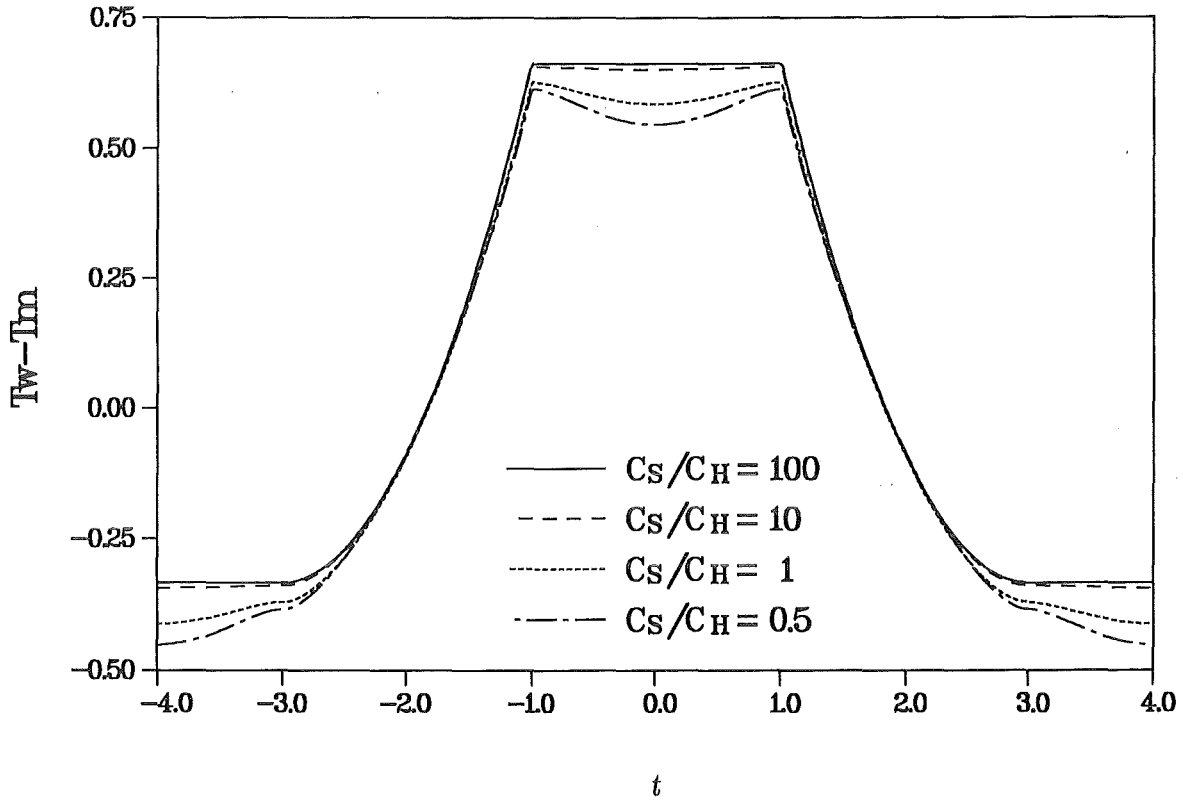

Figure 5.4 *Difference between wall temperature and mean temperature of an MHD flow in a square duct heated by constant planar heat flux $q_n=-e_z$. The thermal conditions are fully developed; $M=1000$.*

5.3 Three-dimensional effects at the entrance of a heated section

Figure 5.5b shows the variation of the wall temperature $T_w(y=0, z=1)$ and $T_w(y=0, z=-1)$ of the heated and adiabatic side wall, respectively, as a function of ξ. Results are shown for a slug-flow velocity profile $u=1$ and for a velocity field typical for MHD flows.

The temperature field is of boundary layer type near $z=1$ for small values of ξ. Thermal disturbances do not extend over the whole cross section. For the case of a slug flow velocity profile the wall temperature grows continuously proportional to $\xi^{1/2}$. For $\xi=O(1)$ thermal disturbances have reached the opposite side wall. Fully developed thermal conditions ($T_w \sim \xi$) are established for larger ξ.

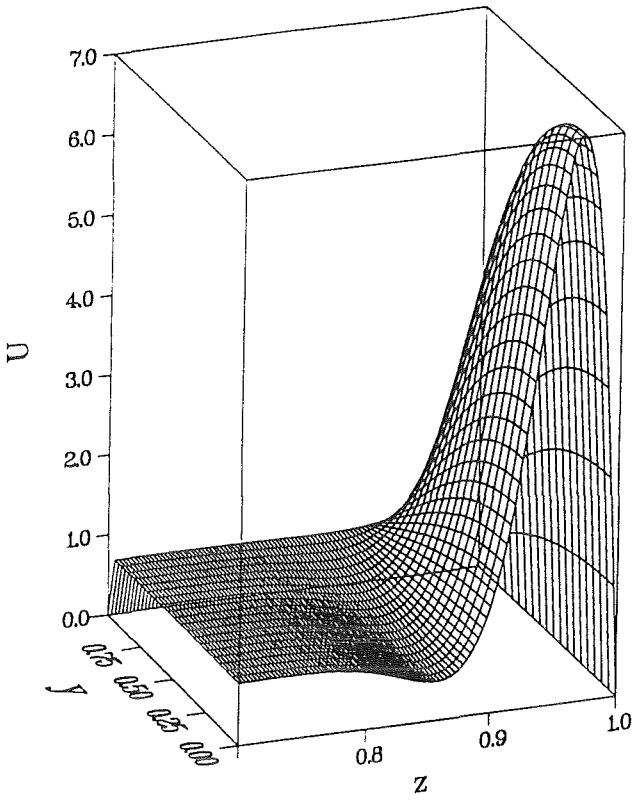

fig. 5.5a

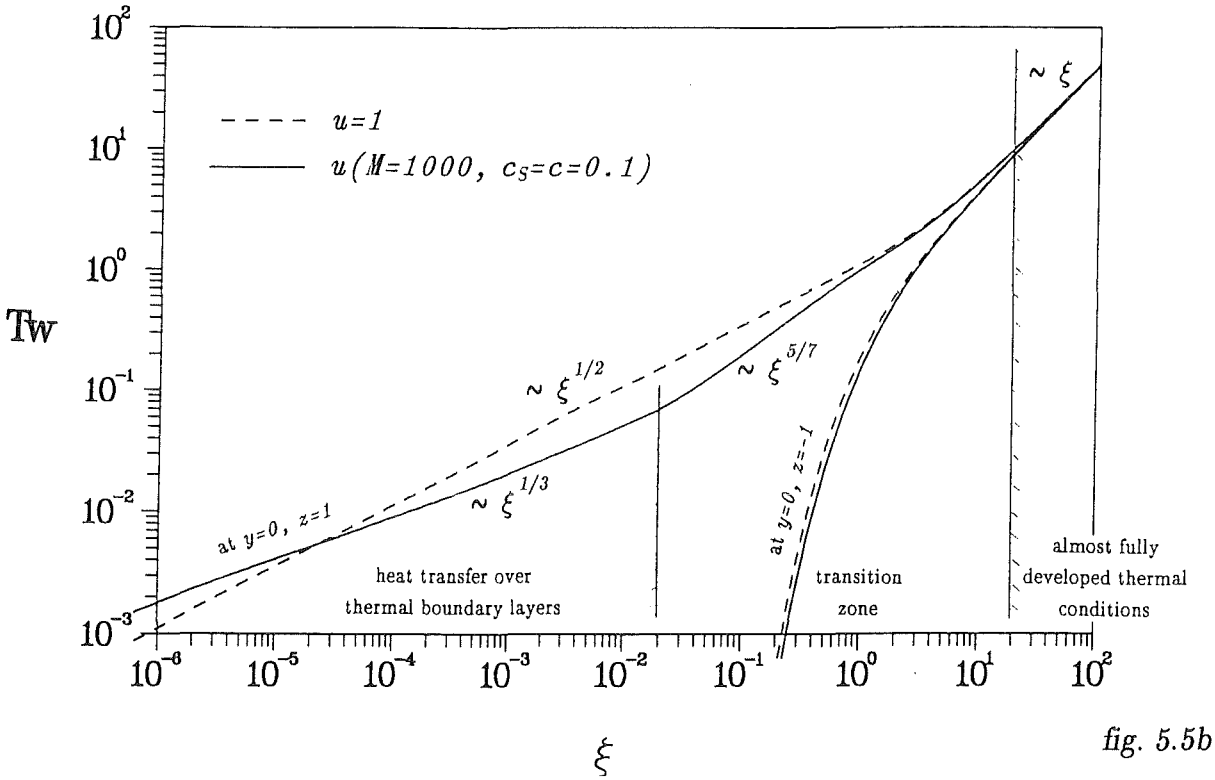

fig. 5.5b

Figure 5.5 Variation of wall temperature at the symmetry plane y=0 with axial length (fig. 5.5b) for bulk flow u=1 and for a typical MHD flow as shown in fig. 5.5a.

For the MHD velocity profile $(M=1000,\ c_S=c=0.1)$ as shown in figure 5.5a the heat transfer conditions are changed. For small values of ξ, when the temperature field is of boundary layer type the heat transfer is governed by two different regimes. The wall temperature first is dominated by $T_w \sim \xi^{1/3}$ corresponding to heat transfer conditions into a fluid with a linearly with the wall distance increasing velocity profile. This regime is the dominant one until the thermal disturbance has reached the position of the velocity peak. The second regime acts upon heat transfer during the spread of temperature through the rest of the cross section. The dependence in this region is $T_w \sim \xi^{5/7}$. Fully developed conditions establish after the disturbance in temperature has reached the other side wall.

The maximum allowable dimensionless wall temperature for the extremely high fusion heat flux is of the order $10^{-2} \div 10^{-1}$. This implies that fully developed conditions for heat transfer are not reached within the total length of a blanket element. To restrict the following discussion of three-dimensional heat transfer to fusion blanket conditions the wall temperature is shown as a function of the axial coordinate ξ only in the relevant range.

The dimension of the computational domain normal to the heated side wall was chosen much larger than the extension of thermal boundary layers. This was done by using a step wise thinner computational domain in subsequent numerical calculations for the same problem, while the temperatures at the border to the bulk of fluid were checked, to ensure that thermal disturbances have not reached these points. Because the wall normal temperature gradient is much larger than the tangential one in extremely thin boundary layers the numerical resolution in the wall normal direction was chosen much higher (for example 400 grid points) than in tangential direction (40 points) to account for these effect. The step width $\Delta\xi$ in axial direction was continuously decreased as $\xi \longrightarrow 0$. This leads to a very good resolution at the entrance of the heated section.

The influence of the velocity profile at the heated side wall on the heat transfer can be seen from figure 5.6. This figure shows the temperature T_w at the fluid wall interface in the middle of the heated side wall (at $y=0,\ z=1$ in figure 5.6a) and at the corner (at $y=1,\ z=1$ in figure 5.6b) as a function of the axial developing length ξ for several ratios c_S/c.

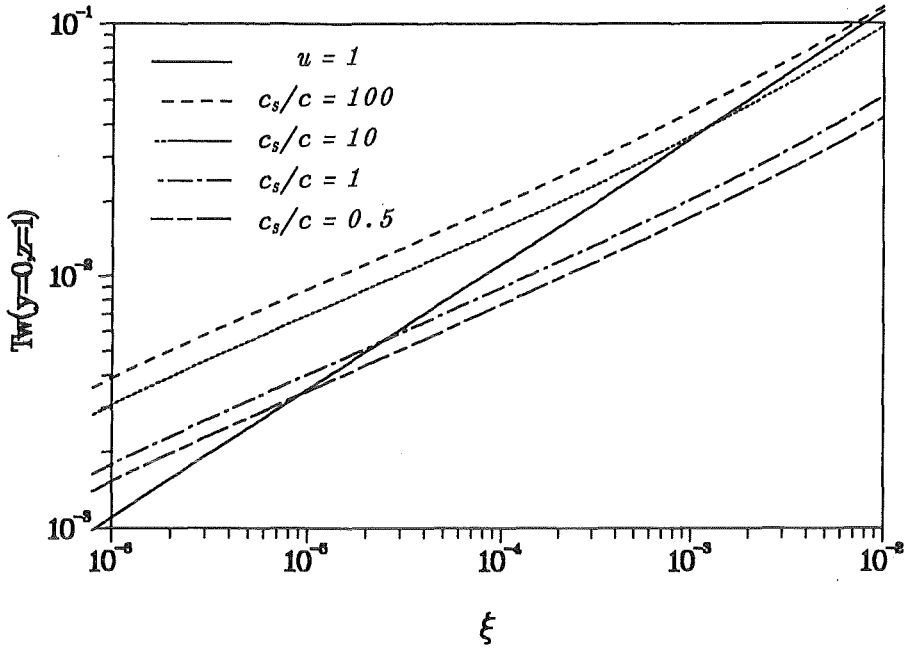

fig. 5.6a

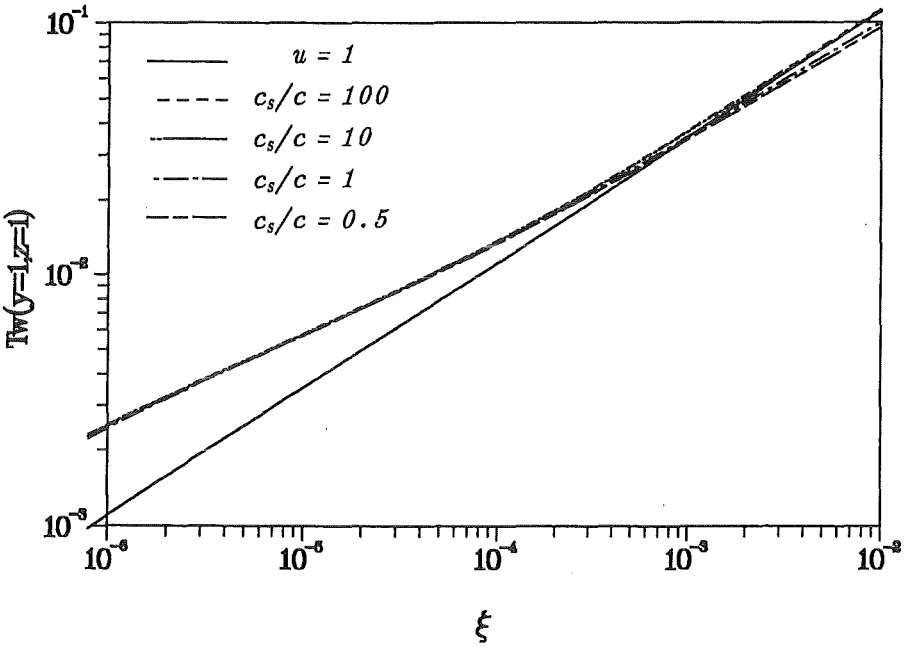

fig. 5.6b

Figure 5.6 *Variation of the temperature of the heated side wall $z=-1$ at the symmetry plane $y=0$ (fig. 5.6a) and at the corner $y=1$ (fig. 5.6b) with axial length for bulk flow $u=1$ and for MHD flows at a Hartmann number $M=1000$ for several ratios c_s/c.*

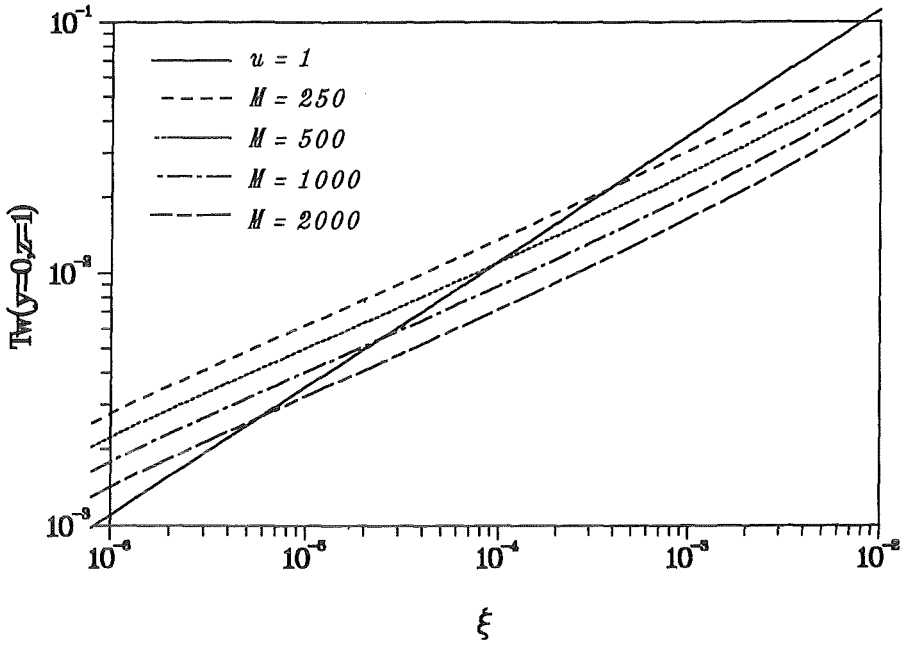

fig. 5.7a

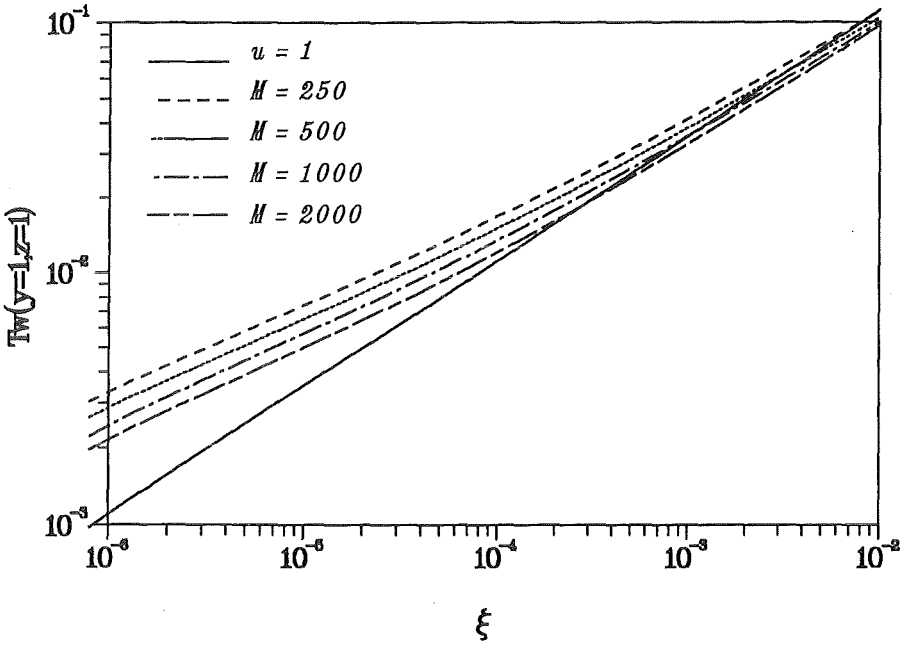

fig. 5.7b

Figure 5.7 *Variation of the temperature of the heated side wall $z=-1$ at the symmetry plane $y=0$ (fig. 5.7a) and at the corner $y=1$ (fig. 5.7b) with axial length for bulk flow $u=1$ and for MHD flows at $c_s/c=1$ for several Hartmann numbers.*

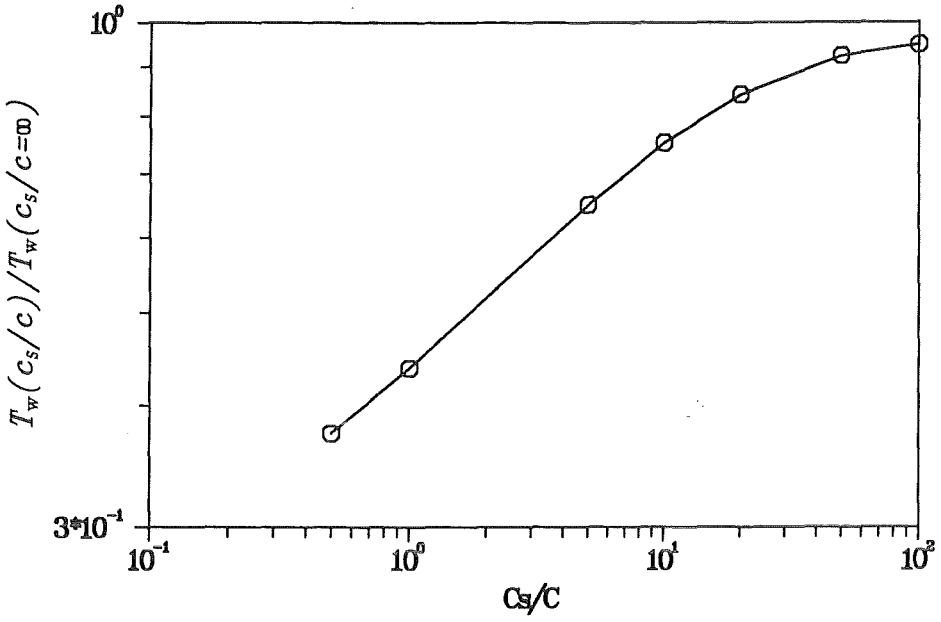

fig. 5.8a

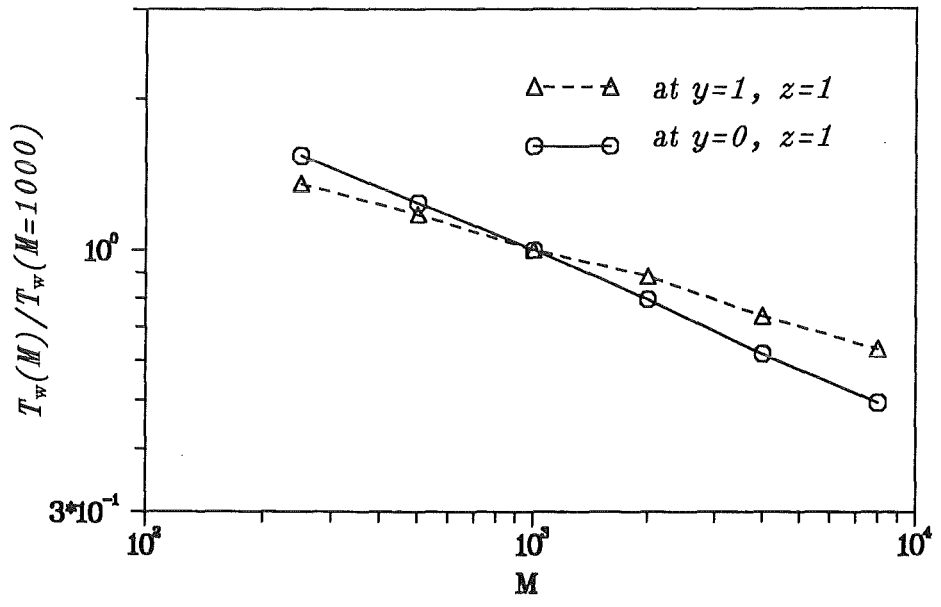

fig. 5.8b

Figure 5.8 *Influence of side wall conductance ratio (fig. 5.8a) and Hartmann number (fig. 5.8b) on wall temperature.*

If there is no jet along the heated side wall $(c_S/c>>1)$ the wall temperature at $y=0$ is higher than at the corner $y=1$. For values of $c_S/c<1$ when pronounced side wall jets occur the convective transport is extremely improved, especially near $y=0$. This leads to an opposite tendency as for large c_S/c. Now the heat transfer is improved near the symmetry plane and the wall temperature is decreased by more than 60%. Near the corner, however, the heat transfer improvement by the jet is only negligible. The corner temperature is approximately independent of c_S/c. Figures 5.6a and 5.6b show that for $c_S/c\leq 1$ or for $c_S/c\geq 10$ the critical (hottest) point in the blanket is either near the corner or near the center of the side wall, respectively.

The influence of the wall conductance ratio c_S on wall temperature at $y=0$, $z=1$ is shown in detail in figure 5.8a. The flow rate in the side layers given by equation $2.4i$ vanishes as $c_S \rightarrow \infty$. For this case the heat transfer is worst. For smaller c_S/c a significant amount of fluid is carried in a thin high velocity jet along the heated wall. This leads to an improved heat transfer with $T_w \sim (c_S/c)^{1/4}$ for $c_S/c<10$.

The influence of the Hartmann number on heat transfer along the heated wall can be seen in figure 5.7. The characteristic dependence along the axial coordinate remains unchanged as the Hartmann number varies from $M=250$ to $M=2000$. Higher values of M lead to thinner jets along the heated wall $(\delta \sim M^{-\frac{1}{2}})$. The fact that for conducting side walls $(c_S>>M^{-\frac{1}{2}})$ the flow rates in these jets are independent of M leads consequently to velocities $u=O(M^{\frac{1}{2}})$ which improve the heat transfer. The wall temperature at the center of the side wall is reduced as $T_w \sim M^{-1/3}$, while the temperature at the corner is decreased only about $T_w \sim M^{-2/9}$ as shown in figure 5.8b.

As overall result of this chapter two formulas are proposed to calculate the wall temperature at the corner $(y=1)$ and at the center of the heated, electrically conducting $(c_S>>M^{-\frac{1}{2}})$ side wall at $z=1$.

$$T_w(y=1, z=1) = 1.2\, M^{-2/9} \cdot \xi^{1/3} \qquad \text{for } \xi M^{\frac{1}{2}} < 2 \cdot 10^{-3}; \quad (5.1)$$

$$T_w(y=0, z=1) = 2(c_S/c)^{1/4} \cdot M^{-1/3} \cdot \xi^{1/3} \qquad \text{for } \begin{matrix} \xi < 10^{-3} \\ c_S/c < 10 \end{matrix}. \quad (5.2)$$

These formulas should provide sufficient information for accurate calculations of wall temperature within, and at least for good estimations beyond the specified application limits. Finally the designer of a fusion blanket should remember that the wall temperatures given by equations 5.1 and 5.2 are the temperatures at the fluid wall interface.

The highest temperature is at the outer wall surface. It can be calculated by the use of the thermal boundary condition *3.2a, b* as

$$T_{wsurface} = T_w + \frac{1}{Bi} \qquad (5.3)$$

6 Other possible applications of the heat transfer code

The numerical code for heat and mass transfer calculations can be applied to any problem with governing equations similar to the general problem *3.4a-c*. Even coupled two-dimensional elliptic problems can be treated when ξ is used as iteration parameter. The solution is reached in the limit $\xi \longrightarrow \infty$. As an example for extended use of the code the numerical solution of a fully developed MHD flow is presented in this chapter.

Fully developed MHD flows are governed by coupled elliptic equations for the velocity component u and for the component of induced magnetic field b (see for example Moreau 1990, p131).

$$\nabla^2 u + M\partial_y b = -1 \,, \qquad (6.1a)$$

$$\nabla^2 b + M\partial_y u = 0 \qquad (6.1b)$$

with boundary conditions

$$u = 0 \,, \qquad (6.1c)$$

$$b + c\partial_n b = 0 \,. \qquad (6.1d)$$

$\nabla^2 = \partial_{yy} + \partial_{zz}$ is the two-dimensional Laplacian in the plane of the cross section. If new variables $\nu_+ = u + b$ and $\nu_- = u - b$ are introduced the equations *6.1a, b* decouple.

$$\nabla^2 \nu_+ + M\partial_y \nu_+ = -1 \,, \qquad (6.2a)$$

$$\nabla^2 \nu_- - M\partial_y \nu_- = -1 \,. \qquad (6.2b)$$

Both equations are of the type of a heat transport equation and can be treated by the previously described numerical code. The coupling between both variables is shifted to the boundary conditions.

$$\nu_+ + \tfrac{1}{2} c\partial_n \nu_+ = \tfrac{1}{2} c\partial_n \nu_- \,, \qquad (6.2c)$$

$$\nu_- + \tfrac{1}{2} c\partial_n \nu_- = \tfrac{1}{2} c\partial_n \nu_+ \,. \qquad (6.2d)$$

They decouple only for insulating channels $(c=0)$.

After these equations have been solved the velocity an induced field are reconstructed.

$$u = \frac{1}{2}(\nu_+ + \nu_-), \quad b = \frac{1}{2}(\nu_+ - \nu_-) . \qquad (6.3a,b)$$

For numerical calculations in rectangular ducts it is sufficient to restrict the computational domain to the region of the parallel layers since all variables do not change with z outside these layers. Results for the variables ν_+ and ν_- and for the velocity component u are shown for different parameters in figures 6.1.

For calculations in circular ducts the Laplacian is given by $\nabla^2 = \partial_{rr} + 1/r\partial_r + 1/r^2\partial_{\varphi\varphi}$ and the derivative in the y-direction by $\partial_y = -\sin\varphi/r\partial_\varphi - \cos\varphi\partial_r$.(see for example Gold 1962). Numerically obtained results for fully developed MHD pipe flows are shown in figure 6.2 for several parameters.

Numerical calculations for MHD flows using velocity u and the electric potential ϕ as variables suffer from poor convergence at very low wall conductance ratios $c<<1$. If in the above introduced formulation c tends to zero the two problems of determining ν_+ and ν_- decouple, convergence becomes independent of c and even better then for $c=O(1)$.

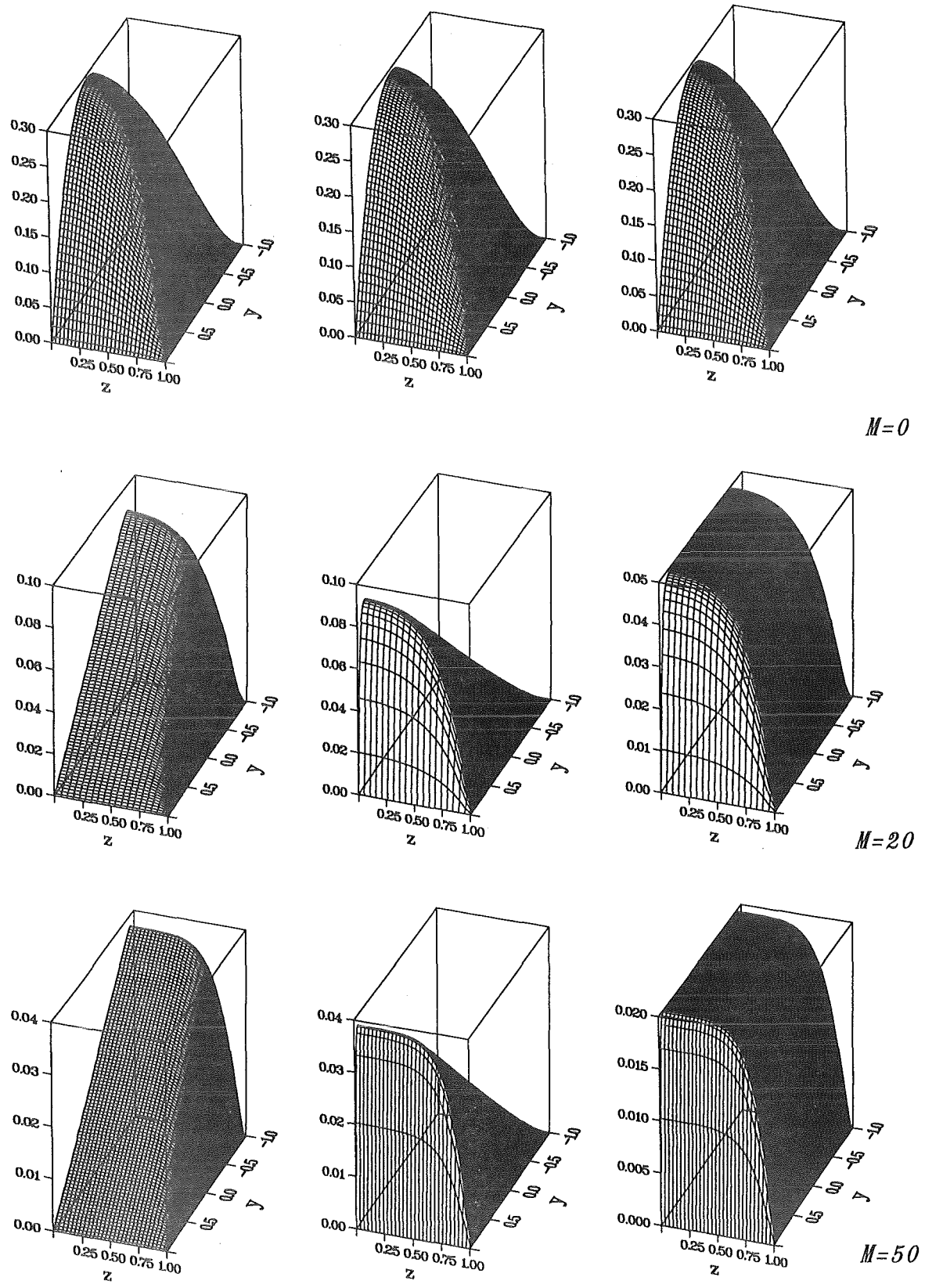

Figure 6.1 *Solution for ν_+, ν_- and $u=\frac{1}{2}(\nu_+ + \nu_-)$ in a square channel with insulating walls $c_s=c=0$ for Hartmann numbers $M=0$, 20, 50.*

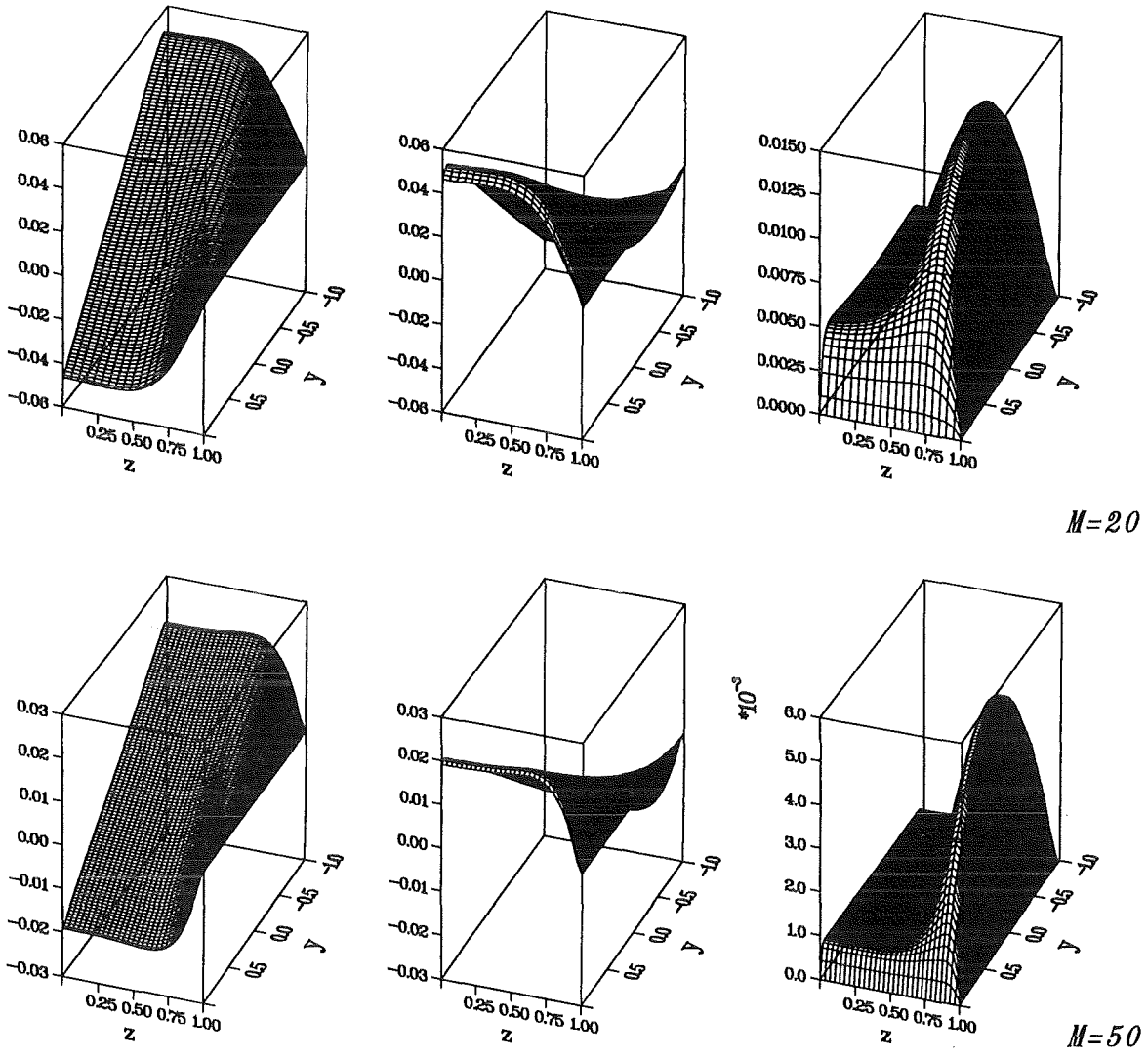

Figure 6.2 *Solution for ν_+, ν_- and $u=\frac{1}{2}(\nu_+ + \nu_-)$ in a square channel with insulating side walls $c_s=0$ and conducting Hartmann walls $c=1$ for Hartmann numbers $M=20,\ 50$.*

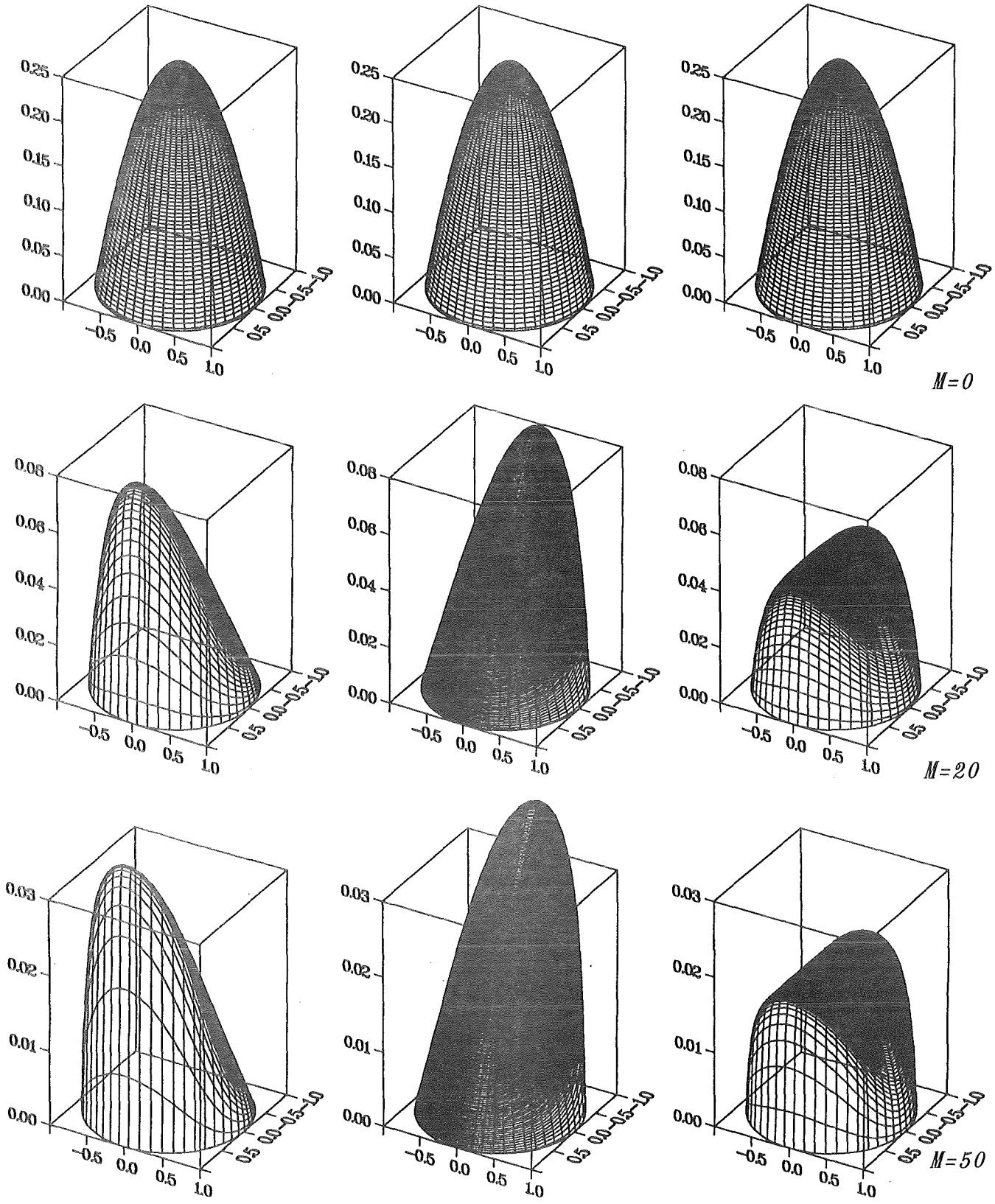

Figure 6.3 *Solution for ν_+, ν_- and $u=\frac{1}{2}(\nu_+ + \nu_-)$ in a circular pipe with insulating walls $c=0$ for Hartmann numbers $M=0,\ 20,\ 50$.*

8 References

Blums, E., Mikhailov, Yu.A., Ozols, R. 1987 Heat and mass transfer in MHD flows; *Utopia Press, Singapore.*

Borgsted, H.U., Röhrig, H.D. 1991 Recent results on corrosion behavior of MANET structural steel in flowing Pb-17Li eutectic; *Jounal of Nuclear Materials* 179-181, 596-598.

Brauer, H. 1971 Stoffaustausch einschießlich chemischer Reaktionen; *Sauerländer, Aarau und Frankfurt a.M.*

Chang, C., Lundgren, S. 1991 Duct flow in Magnetohydrodynamics; *ZAMP* **XII** 100-114

Gardner, R.A. 1968 Laminar pipe flow in a transverse magnetic field with heat transfer; *Int. J. Heat Mass Transfer*, **11**, 1076-1081.

Gold, R.R. 1962 Magnetohydrodynamic pipe flow. Part 1; *J. Fluid Mech.* **13**, 505-512.

Gotovskiy, M.A., Firsova, E.V. 1992 Heat transfer to liquid metal in a tube exposed to a transverse magnetic field; *Heat Transfer Research*, **24**, 2, 226-233.

Hua, T.Q. Picologlou, B.F. 1989 Heat transfer in rectangular first wall coolant channels of liquid-metal-cooled blankets; *Fusion Technology* **15**, 1174-1179.

Kim, C.N., Abdou, M.A. 1989 Numerical method for fluid flow and heat transfer im magnetohydrodynamic flow; *Fusion Technology* **15**, 1163-1169.

Kunugi, T., Tillack, M.S., Abdou, M.A. 1989 Analysis of liquid metal MHD fluid flow and heat transfer using the KAT code; *Fusion Technology* **19**, 1100-1105.

Moreau, R. 1990 Magnetohydrodynaics, *Kluwer Academic Publishers*

Roberts, P.H. 1967 Singularities of Hartmann layers; *Proc.of the Royal Soc. London*, **300**, 94-107.

Walker, J.S. 1981 Magnetohydrodynamic flows in rectangular ducts with thin conducting walls. Part I: Constant area and variable are ducts with strong uniform magnetic fields; *J.de Mechanique* **20**, 79-112.

Ying, A. Lavine, A.S., Tillack, M. 1989 The effect of Hartmann and side layers on heat transfer in magnetohydrodynamic flow; *Fusion Technology* **15**, 1169-1173.

Ying, Tillack, M. 1991 MHD heat transfer in elongated ducts for liquid metal blankets; *Fusion Technology* **19**, 990-995.